NASA-CR-192917

Department of Mechanical Engineering
Penn State University
University Park, PA 16802

Supersonic Shock Wave/Vortex Interaction

IN-02-CR
158616
p-43

by

G. S. Settles and L. Cattafesta

Final Technical Report on NASA Grant NAG-2-575
for the Period April 1, 1989 - September 30, 1992

Submitted to:

Dr. C. C. Horstman, Grant Monitor
NASA-Ames Research Center, MS-229-1
Moffett Field, CA 94035

APRIL 1993

Penn State Gas Dynamics Laboratory
303 Mechanical Engineering Bldg.
University Park, PA 16802

An Experimental Study of Shock Wave/Vortex Interaction

L.N. Cattafesta, III and G.S. Settles
Penn State University, University Park, PA 16802

Abstract

Although shock wave/vortex interaction is a basic and important fluid dynamics problem, very little research has been conducted on this topic. Therefore, a detailed experimental study of the interaction between a supersonic streamwise turbulent vortex and a shock wave has been carried out at the Penn State Gas Dynamics Laboratory. A vortex is produced by replaceable swirl vanes located upstream of the throat of various converging-diverging nozzles. The supersonic vortex is then injected into either a coflowing supersonic stream or ambient air.

The structure of the isolated vortex is investigated in a supersonic wind tunnel using miniature, fast-response, five-hole and total temperature probes and in a freejet using Laser Doppler Velocimetry. The cases tested have unit Reynolds numbers in excess of 25 million per meter, axial Mach numbers ranging from 2.5 to 4.0, and peak tangential Mach numbers from 0 (i.e. a pure jet) to about 0.7. The results show that the typical supersonic wake-like vortex consists of a non-isentropic, rotational core, where the reduced circulation distribution is self-similar, and an outer isentropic, irrotational region. The vortex core is also a region of significant turbulent fluctuations. Radial profiles of turbulent kinetic energy and axial-tangential Reynolds stress are presented.

The interactions between the vortex and both oblique and normal shock waves are investigated using nonintrusive optical diagnostics (i.e. schlieren, Planar Laser Scattering, and Laser Doppler Velocimetry). Of the various types, two Mach 2.5 overexpanded-nozzle Mach-disc interactions are examined in detail. Below a certain vortex strength, a "weak" interaction exists in which the normal shock is perturbed locally into an unsteady "bubble" shock near the vortex axis, but vortex breakdown (i.e. a stagnation point) does not occur. For stronger vortices, a random unsteady "strong" interaction results that causes vortex breakdown. The vortex core reforms downstream of the rear stagnation point, and the reduced circulation distribution once again becomes self-similar in this region. A new model of this interaction is proposed. Finally, a curve defining the approximate limits of supersonic vortex breakdown is presented.

Introduction

The interaction between a supersonic streamwise vortex and a shock wave, henceforth referred to as *shock wave/vortex interaction* (SWVI), is a natural extension of the incompressible vortex breakdown problem. The interested reader is referred to a number of review articles on this topic.[1-3] Incompressible vortex breakdown is known to occur only in highly swirling flows in the presence of an adverse pressure gradient and is characterized by a rapid divergence of the vortex core just upstream of the formation of a stagnation point on the axis of the vortex. The stagnation point is followed by a region of reversed flow of limited axial extent. This definition of vortex breakdown is presumed to be valid in supersonic flow as well.

Background

A supersonic streamwise vortex can be generated, for example, when a vortex sheet shed by a delta wing of a supersonic vehicle flying at a high angle-of-attack rolls up and aligns itself with the freestream velocity vector. This vortex can then interact with the shock system generated by the vehicle, which can affect the aerodynamic performance characteristics of the vehicle.[4] In addition, if a vortex is ingested into a supersonic inlet, the resulting shock wave/vortex interaction can have a negative effect on the inlet performance.[5] Another possible application is the use of the shock wave/vortex interaction to enhance the mixing rate of two coflowing supersonic streams.[6]

The link between shock wave/vortex interactions and supersonic vortex breakdown can be summarized as follows. When a supersonic streamwise vortex encounters a shock wave, the discontinuous pressure rise of the shock wave may be sufficient to burst the vortex. The details of the shock wave/vortex interaction, and whether or not the interaction causes vortex breakdown, depend upon the structure of the vortex. Unfortunately, very little information on the structure of compressible vortices exists in the literature. The studies of Liu[7] and Mandella and Bershader[8], at least, show that there are similarities and differences between incompressible streamwise vortices and their compressible counterparts. Hence, a thorough investigation of shock wave/vortex interactions first requires detailed measurements of the vortex itself.

The structure of shock wave/vortex interactions has been investigated, for example, in a series of Soviet studies using various flow visualization methods.[5,9,10] These studies show that shock wave/vortex interactions result in highly unsteady flow patterns in which the shock wave bulges forward in the upstream direction.

A supersonic vortex breakdown with features similar to those mentioned above has also been observed in supersonic flow over a 75° delta wing at high angle-of-attack[11], as well as behind a Mach disc generated by an overexpanded nozzle.[6,12,13] However, the only detailed quantitative experimental study of shock wave/vortex interactions was carried out by Délery et al.[14], in which five-hole probe and Laser Doppler Velocimetry (LDV) measurements of the vortex and the interaction region downstream of a normal shock were performed. The LDV measurements showed that a stagnation point forms on the axis of the vortex when breakdown occurs. A supersonic vortex breakdown limit curve was also presented by these investigators for the Mach number range 1.6 to 2.28. Unfortunately, no flow visualization results were presented, so that a clear picture of shock wave/vortex interaction phenomenology is not available. Finally, note that computational simulations of shock wave/vortex interactions, although they are still in their infancy and have yet to be validated, exhibit many of the complex features of this problem.[14,15,16]

Objectives

The present study is designed to examine the structure of supersonic streamwise vortices, to investigate the phenomenology of shock wave/vortex interactions, and to extend the supersonic vortex breakdown limit curve to higher Mach numbers. A description of the experimental facilities is presented first, followed by a brief description of the experimental methods and optical flow diagnostics employed. Some representative measurements of supersonic streamwise vortices (in the absence of a shock wave/vortex interaction) are then presented. Next, flow visualization results of shock wave/vortex interaction flowfields produced using three different shock wave generation methods are summarized. Finally, LDV measurements of shock wave/vortex interaction flowfields are presented.

Experimental Facilities

The experiments were conducted in both the Penn State Supersonic Wind Tunnel Facility (PSUSWT) and the Freejet Facility of the Penn State Gas Dynamics Laboratory, depicted in Figures 1(a) and 1(b), respectively. The PSUSWT Facility is an intermittent blowdown tunnel with a 152 mm by 165 mm by 610 mm test section. The 57 m^3, 2 MPa pressure air reservoir provides testing times on the order of 30-60 sec. An asymmetric sliding block nozzle provides a variable Mach number in the range of 1.5 to 4.0. The unit Reynolds number ranges from 65 million/meter at Mach 4 to 100 million/meter at Mach 1.5.

The Freejet Facility is an ambient jet facility that can eject supersonic swirling or non-swirling flows into the atmosphere using the various axisymmetric, method-of-characteristic nozzles described below. The main benefits of this facility compared to the PSUSWT are that it provides essentially-continuous testing times and unlimited optical access. This facility uses as its gas supply either the same air reservoir as the PSUSWT or a set of 43.8 liter, 13.8 MPa bottled gas tanks. A non-venting regulator maintains nearly-constant total pressure conditions in a 50.8 mm diameter stilling chamber. The stilling chamber contains a baffle plate to spread the flow entering from the 19.05 mm inlet pipe, a set of screens for flow conditioning, an inlet from a particle seeder, and a port for measuring the upstream total temperature or total pressure.

This particle seeder consists of a pressure vessel (maximum pressure = 4 MPa) that contains a six-jet atomizer (TSI Model 9306A). The purpose of the seeder is to introduce sub-micron particles into the pressurized stilling chamber for LDV measurement applications. For the current study, the atomizer is filled with 500 ml of either silicon oil (Dow Corning 200 Fluid, 100 cs. viscosity) or a 97.5/2.5 percent-by-volume solution of ethanol and monodisperse polystyrene latex particles (Duke Scientific PSL Microspheres). An external gas supply is required to maintain the seeder at a differential pressure $\Delta p \approx 172$ kPa above the stilling chamber pressure P_{t0}. The atomizer, operating at this differential pressure, thus introduces a fine mist of particles into the pressurized stilling chamber.

There are several ways to generate a supersonic streamwise vortex in these facilities. For example, a delta wing at high angle-of-attack can be mounted in the PSUSWT test section. However, the complex series of shock waves and their reflections from the test section walls make it difficult to isolate the shock wave/vortex interaction. To avoid this complication, a delta wing can be mounted upstream of the wind tunnel converging-diverging nozzle. Unfortunately, the asymmetry of the PSUSWT supersonic nozzle precludes this possibility. Instead a modified version of the supersonic vortex generator used by Metwally[12,13] was employed, as shown in Figure 2. The goal of the supersonic vortex generator is to produce a disturbance-free test rhombus containing well-defined, supersonic streamwise vortices of varying strength and Mach number.

The generator consists of an 18 mm diameter ogive-cylinder forebody mounted on a 9% thick, hollow, bi-convex strut. Supersonic streamwise vortices are generated by injecting regulated, high-pressure gas through the strut into a plenum chamber that contains total temperature and total pressure probes. The injected gas (air for the present tests) is turned parallel to the freestream by a honeycomb flow-straightener. The gas then passes through a converging-diverging (C-D), method-of-characteristics nozzle ($M=2.5$, 3.0, 3.5, or 4.0 for $\gamma=1.4$) containing a set of replaceable swirl vanes immediately upstream of the C-D nozzle. The swirl vanes, depicted in Figure 3, produce a streamwise vortex flow with exit velocity swirl angles of 15°, 30°, 45°, and 60°. The C-D nozzle then accelerates the axial flow but, to first order, does not change the tangential momentum imparted by the swirl vanes. Hence, the combination of swirl vanes and C-D nozzles can produce 16 different supersonic streamwise vortices with tangential Mach numbers ranging from 0 to approximately 1. The swirl-vane/C-D nozzle combinations also attach directly to the stilling chamber of the Freejet Facility.

A schematic of a supersonic streamwise vortex is shown in Figure 4. An observer looking upstream at the nozzle exit would see a vortex whose sense of rotation is counter-clockwise. The helix angle of the streamlines depends on the vane angle and C-D nozzle combination. Note the cartesian coordinate system origin located on the axis of the vortex in the nozzle exit plane. The axisymmetry of the vortex, however, lends itself to a cylindrical coordinate system, which is also shown.

A straight jet can be produced if no swirl vanes are installed ahead of the C-D nozzle. Note that the term "vortex", as used below, refers to a case with swirl, while the term "jet" refers to a case without swirl.

Experimental Methods

Intrusive Probe Measurements

The total temperature, total pressure, Mach number, and flow angle are needed to determine mean-flow quantities in the vortex. The total temperature T_t measurements are accomplished using a fast-response, thermocouple-type probe. A miniature five-hole probe with its pressure transducers mounted very close to the probe tip provides information about the Mach number, total pressure, and flow angle distributions. Figure 5 shows a schematic of the probes along with their pertinent features. Naughton et al.[17] contains a detailed discussion of the five-hole probe (i.e. its design, calibration, implementation, and error analysis). The total temperature and five-hole probe measurements are taken by traversing the probes along the x-direction (see Figure 4 for the coordinate system) at a fixed y and z location until the axis of symmetry is located. Since the vortex is approximately axisymmetric, a single traverse passing through the axis of symmetry sufficiently describes the mean flow.

The Laser Doppler Velocimeter

A key goal of the present work is to make quantitative LDV measurements of supersonic streamwise vortices and shock wave/vortex interactions. However, the large velocities of these flows cause the LDV Doppler frequency to be high, thereby creating the need for a signal processor with a large bandwidth (i.e. > 100 MHz). In addition, it is well known that the LDV signal-to-noise ratio (SNR) is likely to be low for supersonic flows. At the time of the purchase of the LDV system used in this study, only one processor was available commercially that was capable of handling high-frequency, low-SNR signals: the Doppler Signal Analyzer (DSA) made by Aerometrics, Inc. The main features of this system are summarized below (see Cattafesta[19] for a more detailed discussion).

Figure 6 shows a schematic of the LDV system. A 4 W Argon-Ion laser (Coherent Innova Model 70-4) produces a multi-mode, 100:1 linearly polarized, 2 mm diameter beam. Using two plane mirrors with reflection coefficients in excess of 0.99 for the wavelength range of interest, the laser beam is directed into the "fiber drive," which serves three functions. First, a 40 MHz Bragg cell splits the incoming laser beam into higher-order diffracted beams in which the m^{th}-order beam is frequency shifted by $40 \cdot m$ MHz from the unshifted or zero-order beam. The Bragg-cell angle with respect to the incoming laser beam and the acoustic driver signal of the Bragg cell are adjusted to maximize the strength of the $m=0$ and -1 order beams. Second, a dispersion prism splits both the shifted and unshifted laser beams into their component colors. Third, steering mirrors intercept the green ($\lambda=514.5$ nm), blue ($\lambda=488.0$), and violet ($\lambda=476.5$ nm) beam pairs and direct them through optical couplers into six optical fibers (2 μm diameter, single-mode).

For the current study, a 2-D version of the above system is implemented in which the green and blue optical fiber pairs connect to a 2-D transmitter equipped with an achromatic, 500 mm focal-length lens (beam separation = 20 mm). The four laser beams cross at the beam waist such that the two resulting sets of fringes are perpendicular to one another. The green and blue fringes are used to measure the streamwise and swirl velocity components, respectively. The light scattered by the seed particles in the flow is collected by a receiver unit oriented at a 30° forward-scatter angle with respect to the axis of the transmitter. A set of two 200 mm focal-length lenses focuses the scattered light on a 200 μm diameter multi-mode optical fiber, thereby producing an effective probe-volume diameter of 0.4 mm. The collected scatter light is then broken into its component green and blue colors, each color entering its own photomultiplier tube.

Finally, the Doppler frequency is extracted using the Fast Fourier Transform (FFT) capability of the DSA. Each Doppler signal component is appropriately filtered, amplified, and frequency-mixed to produce what is, under optimal conditions, a single-frequency sinusoid. This resulting waveform is next digitally sampled using a 1-bit quadrature method (128 samples at a rate of 160 MHz). The FFT algorithm is then used to extract the Doppler frequency from this discretized signal. The signal is accepted as a valid Doppler burst only if the computed SNR exceeds a user-specified level.

Selected surveys of weak and strong Mach 2.5 vortices are performed in the Freejet Facility. These measurements include radial surveys passing through the axis of symmetry of the vortex at selected z/D locations from the nozzle exit plane. The measurement conditions consist of near perfectly-expanded nozzle flow (to measure the undisturbed vortex) as well as overexpanded nozzle flow (to measure a shock wave/vortex interaction flowfield).

Flow Visualization

The flowfields are visualized using a Z-type Toepler schlieren system. Either a strobed light source (1 μsec exposure at 30 Hz) or continuous light source (Xenon arc-lamp) are used with a horizontal cutoff graded filter as a knife-edge, and the images are recorded using a CCD camera and Super-VHS video cassette recorder.

An additional technique used to visualize the flowfields is the Planar Laser Scattering (PLS) method shown in Figure 7. The laser beam (in this case from a 10 kHz pulsed Cu-Vapor laser rated at a continuous power of 10 W) is formed into a 1 mm thick sheet using a combination of spherical and cylindrical lenses. The sheet cuts through an x-y plane of the flowfield such that it is perpendicular to the z-axis. The vortex is not seeded, but the coflowing supersonic freestream is seeded with sub-micron crystals formed by bypassing the wind tunnel dry air system so that the water vapor in the air crystallizes upon expansion through the supersonic nozzle. The resulting scattered light images are recorded using the same system mentioned above.

Experimental Results

Mean-Flow Measurements of a Mach 3 Vortex

In order to examine the structure of supersonic streamwise vortices and to determine the upstream boundary conditions for the shock wave/vortex interactions, the total temperature and five-hole probes were used to examine the flowfields generated by the vortex generator in the absence of a shock wave/vortex interaction. For these measurements, the nozzle exit pressure was always matched with the freestream static pressure to avoid shock waves.

Figure 8 shows typical component Mach number distributions versus radial distance x from the axis of symmetry of the vortex (in this case for a Mach 3 vortex using the 30° vanes). The vortex core, or the region near the vortex axis where there are large radial gradients, has a radius on the order of 2 mm. The radial Mach number M_x is negligible except in the core, where it is small but negative. This indicates that the radial velocity is directed toward the axis of the vortex. This observation is in agreement with the measurements of Mandella.[8]

The tangential Mach number M_y distribution shows a peak tangential Mach number of about 0.5 for this case, while the axial or streamwise Mach number M_z distribution shows that the vortex has a wake-like axial velocity distribution. Although this feature may be a consequence of the centerbody wake of the swirl vanes, note that the measurements of Délery et al.[14], in which the vortex is generated by a delta wing, show the same wake-like behavior.

Figure 9 shows the nondimensional total pressure $P_t/P_{t,\infty}$ and total temperature $T_t/T_{t,i}$ distributions. (Here, the "i" and "∞" subscripts denote conditions of the injected stream and the flow far from the vortex core, respectively.) Both quantities decrease to minimum values in the vortex core. This decrease is related to the change in entropy, s, as one moves radially inward towards the vortex axis (see Cattafesta[19]). The cause of this feature, commonly referred to as the Ranque-Hilsch effect in the literature[18], is unknown at present. However, Crocco's Theorem

$$\frac{\partial \vec{u}}{\partial t} + \nabla h_o = T \nabla s + \vec{u} \times \vec{\omega} \tag{1}$$

indicates that, for a steady flow, gradients in total enthalpy are related to entropy gradients and vorticity, the former of which is demonstrated in Figure 10.

Using the measured quantities described above, the nondimensional tangential velocity distribution can be calculated and fit to Burgers' tangential velocity profile for an incompressible vortex[2]

$$\frac{V_y}{V_\infty} = \frac{K}{r}\cdot\left(1 - e^{-\left(\frac{r}{r_y}\right)^2}\right) \qquad (2)$$

where K is an indication of the strength of the vortex, and r_y is a characteristic length scale of the streamwise vorticity profile. Figure 11 shows that the nondimensional streamwise vorticity distribution ($\omega_z/\omega_{z,max}$) which is obtained from Eqn. (2), has a Gaussian shape such that at $r = r_y$, $\omega_z/\omega_{z,max} = e^{-1} \cong 0.37$

$$\frac{\omega_z}{\omega_{z,max}} \cong \frac{1}{r}\cdot\frac{\partial(rV_y)}{\partial r} = e^{-\left(\frac{r}{r_y}\right)^2} \qquad (3)$$

Hence, the compressible vortex core is a region of concentrated vorticity and, to within the accuracy of the data, the compressible vortex is seen to have a tangential velocity distribution similar to that of an incompressible vortex.

Hoffmann and Joubert[20] proposed that the nondimensional reduced circulation distribution (i.e. K=radius*tangential velocity) of an incompressible turbulent vortex core has a universal similarity region that consists of three parts: (1) a solid-body region, (2) a logarithmic region, and (3) a transition region between the solid-body and logarithmic regions. Figure 12 shows this nondimensional distribution for the present supersonic vortex cases. In particular, K/K_1 is plotted versus r/r_1, where the subscript "1" denotes the conditions corresponding to the location of the maximum tangential velocity. The data for the three cases shown collapse to a single curve in the solid-body region, transition region, and the logarithmic region up to r/r_1 of about 2. This result strongly suggests that the supersonic streamwise turbulent vortex core, like its incompressible counterpart, has a universal three-layered structure. Note that, for $r/r_1 > 2$, this similarity breaks down.

Figure 13 shows that the nondimensional turbulent kinetic energy (i.e. k/V_∞^2) distribution for the Mach 2.5, 30°-vane vortex is uniform far from the vortex core and rises to a maximum value on the vortex axis. Hence, the turbulence intensity - given by $100(2/3 \cdot k/V_\infty^2)^{1/2}$ - is clearly greatest in the vortex core. Figure 13 also shows the "axial-tangential" Reynolds stress distribution $\langle\langle v_z' v_y' \rangle\rangle / V_\infty^2$ (where the "$\langle\langle\ \rangle\rangle$" denotes a time-averaged quantity). The correlation between v_z' and v_y' is negligible outside the core region (where V_y is small) and increases to a maximum value near the vortex axis where the mean velocity gradients in the radial direction are largest. This result agrees with incompressible streamwise vortex turbulence data (Délery et al.[14]). It should be mentioned that this Reynolds stress distribution is approximately anti-symmetric with respect to the vortex axis; $\langle\langle v_z' v_y' \rangle\rangle / V_\infty^2$ changes sign near x=0 and rises to a maximum value of similar magnitude and radial location on the other side of the vortex.

Flow Visualization of Shock Wave/Vortex Interactions

Three methods for generating a shock wave were examined in detail: (1) generate an oblique shock wave by mounting a 25° wedge in a Mach 4 freestream; (2) generate a normal shock wave by mounting a pitot-type inlet in the test section; and (3) generate a normal shock wave (i.e. Mach disc) by overexpanding the exit flow from the supersonic vortex generator C-D nozzle.

Since shock wave/vortex interactions are thought to depend primarily upon two parameters (vortex strength and shock strength), the interactions can be examined systematically by holding one parameter fixed and varying the other. For all of the cases discussed below, the strength of the shock is fixed by holding the nominal vortex Mach number constant at 2.5. The vortex strength is then varied by changing swirl vanes, and the resulting shock wave/vortex interactions are visualized using the schlieren and PLS techniques. The results for each of the three shock wave generation methods are summarized below.

Oblique Shock Wave/Vortex Interaction

Figure 14 shows a schlieren image of an oblique shock wave/vortex interaction. The dark grid lines are from a 25.4 mm square grid superimposed for reference purposes, and the flow direction is from left-to-right. The nozzle exit appears as the dark rectangle in the upper left corner of the image, and the shock wave generated by the 25° wedge is visible as a dark line in the image. In the vicinity of the vortex core, near the centerline of the vortex generator, the shock wave is perturbed into the shape of a bubble whose size is on the order of the vortex core diameter. This "bubble shock" is observed to be highly unsteady.

In order to investigate this flowfield further, PLS images were taken with the light sheet positioned at various axial locations. Figure 15 shows a PLS image corresponding to a slice of the flowfield at the z location indicated in Figure 14. The plane of the image corresponds to a position just downstream of where the vortex passes through the shock. The shock is visible as a discontinuity in the brightness of the image due to the density increase across it, while the vortex is visible as a dark three-dimensional structure (since the vortex is not seeded).

An oblique shock wave/vortex interaction might be more realistic than a normal shock wave/vortex interaction and does have the added advantage that supersonic flow is maintained downstream of the interaction (so that downstream disturbances do not influence the interaction). However, the disadvantages appear to outweigh the advantages. In particular, oblique shock wave/vortex interactions enable one to consider only moderate strength interactions (compared to normal shock cases). In addition, the interactions produce complex, three-dimensional flowfields as seen in Figure 15 (also see Corpening et al.[15]), the study of which is a daunting chore. Hence, this interaction was not investigated further.

Pitot-Inlet Normal Shock Wave/Vortex Interaction

The second method for generating a shock wave uses a pitot-type inlet with adjustable flaps at its exit to choke the exhaust flow and hold a normal shock near the entrance to the inlet. Figure 16 shows a schematic of the pitot-inlet shock generator mounted in the freestream. The interior of the inlet is 54 mm square, three times larger than the nozzle exit diameter. The shock generator can be positioned anywhere from 0 to 229 mm downstream of the nozzle exit plane.

For the Mach 2.5 case, a change in the structure of the shock wave/vortex interaction occurs when the swirl vanes are increased from 15° to 30°. In particular, the flow visualization results indicate that, as the strength of the vortex is increased, a point is reached where the normal shock bulges forward in the upstream direction to form a bubble shock, the apex of which always intersects the axis of the incoming vortex. Figure 17 shows a schlieren image corresponding to what will be called a "weak interaction", where the shock is located just inside the entrance to the inlet. Figure 18 shows a schlieren image corresponding to what will be called a "strong interaction", where the shock bulges forward in the upstream direction. Note in Figures 17 and 18 that the vortex core is visible as a horizontal line stretching from the center of the nozzle exit to the shock generator.

In the weak interaction generated by the 15° vanes, the shock shape is perturbed slightly into the shape of a bubble whose characteristic size is on the order of the incoming vortex core diameter. The interaction is unsteady and, as was the case with the oblique shock wave/vortex interaction, the bubble shock always bulges forward in the upstream direction.

In the strong interaction generated by the 30° vanes, however, the size of the bubble shock and the distance it propagates in the upstream direction increase by an order-of-magnitude. Again, the flow is highly unsteady.

The inlet normal shock generator has both advantages and disadvantages. Considering the advantages first, it produces a shock of semi-infinite extent which is an order-of-magnitude larger than the vortex core diameter. Second, it shows a distinct change in the flow structure as one proceeds from a weak interaction to a strong interaction. Its disadvantages are, first, that it is susceptible to influence from downstream disturbances since the flow behind the normal shock is subsonic. Second, this configuration, like that of the wedge, has restricted optical access. Hence, measurements in the interaction region are difficult to make.

Overexpanded Nozzle Shock Wave/Vortex Interaction

The last shock-wave generation method examined uses an overexpanded nozzle exit condition to generate a Mach disc. In particular, the exit pressure of the injected flow is mismatched with the freestream static pressure, which causes a conical oblique shock to cross irregularly and produce a Mach disc. The total pressure of the injected stream controls the size and location of the Mach disc for fixed tunnel freestream conditions.

In a similar fashion to that described above, the strength of the vortex was increased while the nominal strength of the shock was held constant. For the weak interaction cases, the normal shock suffers an unsteady perturbation of its shape and distorts once again into the shape of a bubble. This bubble shock bulges forward in the upstream direction and has a characteristic size on the order of the incoming vortex core diameter. A schlieren image of a weak interaction generated by the 15° vanes is shown in Figure 19.

When the 30° vanes are used to increase the strength of the vortex, a strong interaction, first observed by Metwally[12,13], is seen as shown in Figure 20. The extent to which the shock propagates upstream is again larger than the vortex core diameter. A new feature of this interaction, and that which clearly distinguishes the weak interaction from the strong interaction, is the appearance of a new shock wave downstream of the initial shock. As shown in Figure 21, Metwally proposed that the initial shock is strong enough to burst the incoming vortex, causing the formation of a stagnation point and a recirculation region. The flow must expand around the recirculation region and then recompress. This is accomplished by a recompression shock as shown in Figure 21. Although plausible, this flow model remains to be validated.

Are the two normal shock wave generation methods equivalent? The difference in flow structure is apparently due to different downstream boundary conditions. That is, the flow downstream of the inlet shock generator is subsonic, while the flow downstream of the overexpanded nozzle case accelerates to supersonic conditions. Otherwise, the shock structure is similar in that both methods produce unsteady bubble shocks. In addition, the same set of conditions that causes a transition from the weak interaction to the strong interaction for the pitot-inlet case also causes this transition for the overexpanded nozzle case. Only the scale of the interactions is different. Therefore, it appears that the methods are essentially equivalent.

The advantages of the overexpanded nozzle make it the method of choice. First, the fact that supersonic flow is recovered downstream of the interaction means that downstream disturbances will not affect the interaction region. Second, the overexpanded nozzle case provides the easiest access for quantitative measurements of the shock wave/vortex interaction region. Third, the appearance of a recompression shock clearly distinguishes the strong interaction from the weak interaction.

One possible disadvantage of this method is that the limited size of the Mach disc may impose an extraneous length scale on the shock wave/vortex interaction (in addition to the incoming vortex core diameter) which can possibly affect the detailed structure of the interaction. As just noted, this possibility does not influence the weak-to-strong interaction transition. Nonetheless, it does warrant further investigation.

Instantaneous PLS Images

In order to investigate further the shock wave/vortex interaction, instantaneous PLS images of the overexpanded nozzle shock wave/vortex interaction were obtained in the Freejet Facility, in which the Mach 2.5 flow (jet or vortex) was exhausted to ambient conditions. In this experiment, a laser light sheet approximately 1 mm thick is positioned in the y-z plane so that it cuts through the axis of symmetry of the vortex. The light-scattering particles are ethanol crystals that are formed when the ethanol vapor crystallizes upon expansion through the supersonic nozzle. (The particles produce nearly 100% polarized light at a 90° scattering angle when a parallel, unpolarized white light beam is passed through the flow; this means that the particles are very small compared to the wavelength of the incident white light and approach the Rayleigh scattering limit.) The scattered light produced by the ethanol crystals is recorded at a 90° scattering angle using the system described earlier, and the images are subsequently processed using an image processing system.

Figure 22 shows an instantaneous image generated by an Nd-YAG laser pulse for the Mach-disc jet case, where the planar Mach disc is clearly visible. The dark region downstream of the Mach disc occurs because the temperature rise across the normal shock is larger than that associated with the two oblique shocks. Hence, the ethanol crystals only melt upon passing through the normal shock. Figure 23 shows a similar image for the weak interaction case, while Figure 24 shows an image of the strong interaction case. Figures 23 and 24 reveal considerable detail never before seen in a shock wave/vortex interaction. The vortex core appears dark in both images upstream of the shock because of its lower seeding density. For the weak interaction case in Figure 23, a perturbation in the normal shock shape is seen. For the strong interaction case in Figure 24, note that the bubble shock bulges forward and intersects the vortex axis just as seen in the earlier schlieren images. When the bubble shock intersects the vortex axis, the vortex core diverges rapidly. This is a known characteristic of incompressible vortex breakdown[21] that, to the best of our knowledge, has not been observed previously in supersonic flow. In addition, note the increased intensity of scattered light immediately downstream of the bubble shock. The fact that the vortex core, which was dark before the shock, is brighter immediately downstream of the shock suggests that scattering particles from the outer non-swirling flow have been entrained into the core by way of a local flow reversal. Hence, the structure revealed in this figure supports the Metwally and Settles flow model shown in Figure 21. Non-intrusive velocity measurements of the weak and strong interactions that validate this claim are discussed below.

LDV Measurements of the Overexpanded-Nozzle SWVI

This section describes the results of the LDV measurements of the weak and strong SWVI. First, a statistical method is presented for analyzing the results of velocity measurements in an unsteady region to determine whether or not vortex breakdown has occurred in either the weak or the strong interaction. This is followed by a discussion of the results for the weak and strong interactions, respectively, in the unsteady region and then downstream of the interaction where the mean flow is once again steady.

LDV Measurements of the SWVI in Unsteady Regions

The flow visualization results show that the SWVI flowfields are characterized by unsteady shock motion. In the weak interaction, this unsteadiness is confined to the immediate vicinity of the Mach disc, while the unsteady region is much larger for the strong interaction. How does this unsteadiness affect velocity measurements using LDV? Aside from problems that arise due to the refraction of the laser beams by moving shock waves, the main difficulty is that the probe volume is fixed in space while a fluctuating shock wave moves about this fixed location. Depending on whether the probe volume is located upstream or downstream of the shock at a given instant in time, the measured velocity is either supersonic or subsonic, respectively. Hence, it is reasonable to expect that a velocity histogram resulting from many samples at a given measurement location will have at least a bimodal velocity probability density function (PDF).

Figure 25 shows an example of such a situation, where a histogram of the axial velocity V_z measurements is shown for a point located in the "heart" of the strong SWVI. The bimodal distribution shows two primary "states"; one corresponds to supersonic flow conditions, and the other corresponds to subsonic reversed flow. The physical significance of the mean velocity for this particular situation, which lies somewhere between these two peaks, is questionable. Nevertheless, a goal of the measurements in the unsteady region is to identify a stagnation point and a reversed flow region.

To accomplish this, the following approach is adopted for the initial LDV measurements designed to determine if vortex breakdown occurs in either the weak or strong interaction. Two-dimensional, coincident velocity measurements of tangential and axial velocity are obtained in the (y,z) plane containing the vortex axis (see Figure 1(b) for the coordinate system). To determine if a stagnation point and a recirculation region exist in the interaction, the probability that $V_z \leq 0$ is determined from the number of velocity samples at a point,

$$P(V_z \leq 0) = \frac{\text{Number of Samples with } V_z \leq 0}{\text{Total Number of Samples}} \tag{4}$$

where the total number of samples is typically 500 points. Clearly, the higher the value of $P(V_z \leq 0)$, the higher the percentage of the time that a reversed-flow state exists at a given measurement location. A contour plot of $P(V_z \leq 0)$ for a series of measurement locations in a plane then indicates whether or not a recirculation region exists and, if so, determines its approximate size. (Note that the *proper* way to quantitatively examine such an unsteady region is to use conditional sampling, in which data are taken only when the shock is in a particular position. However, such a scheme is very complex and is beyond the scope of the current study.)

LDV Measurements of the Weak SWVI

The schlieren flow visualization results are used to obtain the appropriate locations for velocity measurements in the weak interaction region. Figure 26 shows the measurement locations superimposed as a grid on a time-averaged schlieren image (16.6 msec) of the weak SWVI. As seen in the image, the time-averaged motion of the small bubble shock is averaged out, leaving essentially a Mach disc. The measurement locations are therefore clustered in this vicinity.

The results show that no stagnation point or reversed axial flow region exists for this flow. That is, $P(V_z \leq 0)$ is zero for the weak SWVI. Using the definition that vortex breakdown corresponds to the formation of a stagnation point followed by a reversed flow region, it is concluded that the weak interaction does not cause vortex breakdown.

If this interaction does not cause supersonic vortex breakdown, then what happens to the vortex structure downstream of the Mach disc? In particular, how are the axial and tangential velocity profiles modified, if at all? To address this issue, two-component, coincident velocity measurements of V_y and V_z along the x-direction are obtained for fixed y- and z-locations. The y-location corresponds to the y-location of the vortex axis at the nozzle exit plane ($z=0$), while the z-locations (5.08 and 6.35 mm) are approximately 0.5 mm and 1.8 mm, respectively, downstream of the Mach disc. Note that downstream of the Mach disc, Gaussian PDF's are obtained so that the concept of a mean velocity is justified.

Figure 27 shows the measured axial velocity profiles versus "radial" distance x from the vortex axis of symmetry. Since the time-averaged schlieren image of Figure 26 shows a Mach disc, the shock relations are used to jump across the normal shock by assuming that (1) the upstream velocity V_1 is equal to the local axial velocity at $z=0$ and (2) the total temperature T_t is constant with respect to x at 291 K (which is reasonable for this weak-vortex case). The agreement between the LDV data 0.5 mm downstream of the shock and the calculated velocity V_2 just downstream of the shock is good, the slight discrepancy being due to particle lag. Note that the location of the slip line generated at the triple-shock intersection, shown in Figure 27, agrees with the schlieren image of Figure 26. The V_z profiles downstream of the shock show that the flow is accelerating slightly. This result also agrees with the schlieren image in Figure 26, which shows the presence of shock waves further downstream (indicating that a reacceleration to supersonic speed has occurred).

Figure 28 shows the "tangential" velocity profiles V_y at $z=0$, 5.08, and 6.35 mm, respectively. The region contained between the slip lines clearly shows that the tangential velocity distribution (and hence, the streamwise vorticity profile) is unchanged by the normal shock wave. This is an expected result since the component of velocity tangent to a shock is invariant across the shock wave.

LDV Measurements of the Strong SWVI

For the strong interaction, two different cases are considered: (1) a "small" Mach disc that is about 4.5 mm in diameter (i.e. 0.25•D where D is the nozzle exit diameter) and (2) a "large" Mach disc that is about 9 mm in diameter (i.e. 0.5•D). These different-diameter Mach discs help to determine what effects the Mach-disc size has on the structure of the interaction. The results of LDV measurements for both the small and the large Mach-disc cases are considered below.

A. The Small Mach-Disc Case

In a similar fashion to the weak SWVI, the schlieren flow visualization results are used to obtain the appropriate locations for velocity measurements in the interaction region. Figure 29 shows the measurement locations superimposed as a grid on a time-averaged schlieren exposure (16.6 msec) of this SWVI. In addition, contours of $P(V_z \leq 0)$ are shown, where the outermost contour is the 5% level and the $P(V_z \leq 0)$ increases to a maximum value of 30% in the center of the contours.

This important result verifies that the strong SWVI does cause vortex breakdown. As mentioned above, these contours are expected to be representative of the extent of the recirculation region. If this is true, then the furthest upstream extent of the recirculation region (which is seen to be axisymmetric) is about 6 mm from the nominal location of the Mach disc, while the furthest downstream extent is about 2 mm from the nominal Mach-disc location. The radial extent of the recirculation region is only about 2 mm, so that the recirculation region appears to have the shape of an ellipse that has its major axis parallel to the vortex axis.

What happens to the vortex structure just downstream of the interaction, where the mean flow is "steady" (i.e. Gaussian velocity distributions are obtained)? Figure 30 shows the axial velocity profiles versus radial distance at z-locations = 0, 10.16, and 11.43 mm downstream of the nozzle exit plane. These profiles indicate that the axial velocity is approaching the sonic velocity (about 312 m/s for T_t=291 K); the flow visualization results (which showed shock waves downstream of the interaction) presented in Cattafesta[19] support this contention.

Figure 31 shows the V_y profiles downstream of the interaction compared with the upstream profile. The maximum tangential velocity has increased by about 20%, while the core diameter (i.e. the distance between the local maxima in the V_y profile) has decreased slightly from 3 mm to 2.3 mm. These results contrast with the findings of Délery et al. (1984), who report a *decrease* in the maximum tangential velocity and an *increase* in the vortex core diameter (for an inlet-generated normal SWVI).

The discrepancy exists because what happens to the downstream vortex structure depends upon the downstream boundary conditions imposed by the interaction and, as will be shown in the next section, the size of the Mach disc. To see this, consider the inlet-generated normal shock wave/vortex interaction of Délery et al. Their LDV data showed that, for a case corresponding to vortex breakdown, a large recirculation region is formed, thereby causing a significant deflection of the incoming streamlines. Hence, it is not surprising that the vortex core enlarges and that the tangential velocity decreases (assuming that angular momentum is conserved).

In the current small-Mach-disc case, a recirculation region also exists. However, the radial extent of this slim elliptically-shaped recirculation region is probably much less than that of the inlet case (see Figure 18). If this is true, then the deflection of the flow imposed by the current recirculation region is much smaller than in the inlet-shock case. In addition, according to the model of the strong overexpanded-nozzle case by Metwally et al.[12], the flow expands around the recirculation region and is turned back to the horizontal direction by the recompression shock (see Figure 21). Therefore, if the net turning angle of the flow is zero, then the vortex core diameter and tangential velocity will remain essentially unchanged. The reason for the slight change in both of these quantities, seen in Figure 31, is explained below.

B. The Large Mach-Disc Case

Figure 32 shows contours of $P(V_z \leq 0)$ for the large Mach-disc case superimposed as a grid on a 16.6 msec schlieren image of the interaction. Note that the front part of this interaction is located just inside the nozzle exit where the nominal conditions upstream of the interaction are assumed to be the same as for the small Mach-disc case. The velocity measurements, the locations of which are indicated in Figure 32, capture the latter part of the recirculation region only, as represented by the probability contours. Thus, over the range of sizes considered, the Mach-disc size does not affect whether or not vortex breakdown occurs, although it does affect the size of the recirculation region.

Figures 33 and 34 show the V_z and V_y profiles, respectively, along with their corresponding upstream profiles. Again, Figure 33 shows that the axial flow rapidly approaches the sonic velocity of 312 m/s. In addition, Figure 34 shows that the tangential velocity profile is unchanged when the vortex passes through the shock wave, unlike the small Mach-disc case.

A comparison between the V_y profiles of the two Mach-disc cases clearly shows that the size of the Mach disc affects the downstream structure of the vortex. A possible explanation is that the small-diameter (4.5 mm) Mach disc is comparable in size to the diameter (3 mm) of the vortex core, while the large-diameter (9 mm) Mach disc is much larger than the incoming vortex core diameter. Hence, for the small Mach-disc case, the slip line generated at the triple-shock intersection is too close to the vortex core and therefore affects the tangential velocity distribution.

Indeed, a close inspection of Figure 22 reveals that the slip line is directed not horizontally but towards the z-axis at about a 10° angle (which is reasonable since the flow is accelerating in this region). Thus, the net radially-inward deflection of the flow by the triple-shock system may explain why the vortex core diameter decreases slightly for the small Mach-disc case. In order to conserve angular momentum, the tangential velocity must increase. For the large Mach-disc case, however, the triple-shock system is far enough away from the vortex core so that the vortex core diameter and hence, the tangential velocity profile, are largely unaffected.

Supersonic Vortex Breakdown Limit Curve

The results of the LDV measurements show that only the "strong" SWVI causes vortex breakdown. Thus, the data obtained from the mean flow measurements may be used to construct a supersonic vortex breakdown limits curve. That is, the tangent of the maximum flow angle in the vortex, $\tan(\theta_{max})$, represents a local measure of the incoming vortex strength, while the corresponding value of the axial Mach number M_z at the location of θ_{max} represents the shock strength. (Note that, for vortices oriented with their axis-of-symmetry perpendicular to the plane of a shock wave, M_z equals the component Mach number that is normal to the shock, M_n.) Since the Reynolds number of these vortices is high and does not vary greatly, then a supersonic vortex breakdown limits curve can be constructed (Délery et al.[14]).

Figure 35 shows this supersonic vortex breakdown limits curve or region, where the vortex strength, $\tan(\theta_{max})$, is plotted versus shock strength M_n. The data of Délery et al. are included for comparison. The open symbols represent the measured weak-interaction (no-breakdown) cases, while the closed symbols represent the measured strong-interaction (breakdown) cases. The data of the current study agree qualitatively with the data of Délery et al., in that there clearly exists an inverse relationship between the vortex strength and shock strength required to cause supersonic vortex breakdown. These data are useful because they allow one to determine if a supersonic vortex of a given strength will burst when it encounters a shock wave of a particular strength.

The dotted line that passes through the entire data set is an approximate criterion for vortex breakdown determined as follows. For the following analysis, assume that the radial velocity in the vortex is negligible and that the vortex axis is normal to the plane of the shock wave (as mentioned above).

Normal shock theory dictates that V_t is invariant across the shock, while the normal velocity ratio across the shock is given by

$$\frac{V_{n,2}}{V_{n,1}} = \frac{(\gamma - 1) M_{n,1}^{\ 2} + 2}{(\gamma + 1) M_{n,1}^{\ 2}} \tag{5}$$

where "1" and "2" denote conditions upstream and downstream of the shock, respectively, and $\gamma = 1.4$ for the air data presented here.

Since the normal velocity component is decreased and V_t is unchanged, the nondimensional vortex strength effectively increases upon passage through the shock. The ratio of the downstream vortex strength, τ_2, to the upstream vortex strength, τ_1, is thus given by the relation

$$\frac{\tau_2}{\tau_1} = \frac{(\gamma + 1) M_{n,1}^{\ 2}}{(\gamma - 1) M_{n,1}^{\ 2} + 2} \tag{6}$$

where $M_{n,1} = M_1 \cos(\theta)$ and $\tau = V_t / V_n$, following the definition of Délery et al. (Note that, when the radial velocity is negligible, $\tau_1 = \tan(\theta_{max})$.)

If Eqn. 6 is fit to the data shown in Figure 35 (except for the point near $M_n = 2$ where $\tau_1 \approx 0.4$) using a least-squares method, then a best-fit value for τ_2 is found to be ~ 0.6. Eqn. 6 is shown plotted in Figure 35 and fits the data reasonably well. The breakdown curve is extended beyond the existing data to $M_n = 1$ and to $M_n \rightarrow \infty$, where the curve asymptotes to a constant value of ~ 0.1. This is discussed below.

Eqn. 6, which serves as an approximate supersonic vortex breakdown criterion, has a physical basis borrowed from incompressible vortex breakdown theory. Simply stated, when the maximum flow angle of the vortex exceeds a critical value, $\tan^{-1}(0.6) \approx 30°$ according to the current data, vortex breakdown is likely to occur. Note that a typical maximum flow angle of 40° is often quoted as being required for incompressible vortices to burst in the absence of an externally-imposed adverse pressure gradient (Hall[22]).

While the current 30° limit, corresponding to the still-compressible case of $M_n = 1$, does not agree with the incompressible limit, it does indicate that the strength of a vortex cannot be increased without bounds if the vortex is to remain stable (i.e. not break down). Note that the case $M_n=1$ corresponds to a shock of zero strength and is therefore equivalent to a zero (externally-applied) adverse pressure-gradient case. Whether or not the criterion is accurate in this region obviously requires additional data beyond the present scope.

At large Mach numbers, the normal velocity ratio across a shock asymptotes to a value of 6 for $\gamma=1.4$. Thus, the vortex strength can, at most, increase by a factor of 6 due to its passage through a normal shock. As a result, a hypersonic air vortex apparently requires a maximum flow angle in excess of about 5° or it will not burst under the influence of any shock wave. Once again, additional data at higher Mach numbers are needed to determine if this estimated magnitude is indeed correct, though it appears that the criterion makes physical sense. Note that the breakdown criterion of Eqn. 6 is extrapolated here with extreme caution; it is done mainly to examine whether or not the curve fit is physically realistic at its extreme limits rather than to determine any specific breakdown limits outside the range of the data.

A Flowfield Model of the Strong SWVI

The last section of this report proposes a flowfield model of the overexpanded-nozzle SWVI. The model combines the flow visualization results with the quantitative LDV measurements just presented. Given the complexity of SWVI flowfields, the model is not expected to embody a comprehensive explanation of the phenomenon. Rather it illustrates the flowfield structure at its present level of understanding.

The LDV measurements show that the model of Metwally et al.[12] captures the essence of the interaction in a time-averaged sense with the following modifications, as shown in Figure 36(a). The vortex core reforms downstream of the recirculation region. The size of the downstream core and the extent to which the tangential velocity distribution is changed depend upon the Mach-disc diameter. If the disc diameter is large compared to the incoming vortex core diameter (i.e. a semi-infinite normal shock case), then the vortex core diameter and tangential velocity distribution are unchanged downstream. Figure 36(b) shows a schematic corresponding to this ideal case where the vortex bursts upon passing through a semi-infinite normal shock. Future work should examine more closely the role of the Mach-disc size on the detailed structure of the interaction.

How can the observed unsteadiness be explained? The unsteadiness of this interaction is not periodic. Rather, it is random (see Cattafesta[19] for more detail) and may be due to the motion of the forward stagnation point along the vortex axis. It is well known that incompressible vortex breakdown is characterized by large axial movements of the breakdown point, since this position is especially sensitive to downstream disturbances. If, as it appears in the PLS images of SWVI described earlier, the vortex bursts just downstream of the tip of the bubble shock, then the large range of motion of the bubble shock (compared to the other shock waves) can probably be attributed to axial movement of the breakdown point. Characterization of both the turbulence and the shock motion spectra may provide a better understanding of this unsteadiness.

Finally, the flow visualization results show that the instantaneous structure of this interaction undergoes large excursions from its mean structure. Future work should therefore examine quantitatively the instantaneous structure of the recirculation region for different positions of the bubble shock. This can be accomplished experimentally (although it would be quite a task) using the conditional-sampling technique mentioned earlier.

Conclusions

Experiments on shock wave/vortex interactions have been performed using the combination of a supersonic streamwise vortex and various shock wave generation methods. The flowfields were investigated using total temperature and five-hole probe surveys, as well as the non-intrusive LDV, schlieren and PLS imaging techniques. Representative mean-flow measurements show that the supersonic streamwise vortex has a similar tangential velocity and, hence, streamwise vorticity profiles to its incompressible analog. There are differences, however, between the compressible case and incompressible case. For example, the compressible vortex possesses a total temperature deficit and a wake-like axial velocity profile in its core not found in an incompressible vortex upstream of breakdown.

The turbulence measurements (of $V_y \approx V_t$ and V_z) show that the vortex core is a region of significant turbulent fluctuations. The turbulent kinetic energy rises to a maximum value on the vortex axis and asymptotes to a constant value far from the vortex axis. The axial-tangential Reynolds stress correlation reaches a peak value in the solid-body region, in which the velocity gradients are largest, and decreases to zero near $r=0$ and as $r \to \infty$ (where the velocity gradients are approximately zero at these locations). Both of these distributions are approximately symmetric with respect to the vortex axis of symmetry.

Various shock generation methods were examined in detail (a wedge-generated oblique shock, a pitot-inlet-generated normal shock, and an overexpanded nozzle Mach disc). The resulting interactions were investigated using non-intrusive flow diagnostics. The overexpanded nozzle Mach disc was found to be the method of choice, primarily because of its simplicity and easy optical access for measurements in the interaction region.

The shock wave/vortex interactions were found to be highly unsteady regardless of the incoming vortex strength. Two regimes were discovered: (1) a weak interaction characterized by the perturbation of the main shock into a bubble shock that bulges forward in the upstream direction with a characteristic size on the order of the incoming vortex core diameter, and (2) a strong interaction characterized by a bubble shock which is much larger than the incoming vortex core diameter. For the case of the overexpanded nozzle flow, the strong interaction is further distinguished from the weak interaction by the formation of a secondary recompression shock downstream of the bubble shock. Instantaneous PLS images and LDV measurements show that only the strong interaction corresponds to supersonic vortex breakdown.

The supersonic vortex breakdown limit curve of Délery et al. was extended from approximately Mach 2.5 to 4. The present data agree qualitatively with those of Délery in that the strength of a shock required to burst a supersonic streamwise vortex is inversely related to the vortex strength. An approximate vortex breakdown criterion is presented.

Acknowledgements

This work is supported by NASA Grant NAG 2-575, monitored by Dr. C.C. Horstman of NASA-Ames Research Center. We further thank J.D. Miller, Dr. J.W. Naughton, and Dr. E. Stanewsky for their assistance.

References

1. Hall, M.G., "Vortex Breakdown," *Annual Review of Fluid Mechanics*, Vol. 4, pp. 195-218, 1972.
2. Leibovich, S., "The Structure of Vortex Breakdown," *Annual Review of Fluid Mechanics*, Vol. 10, pp. 221-46, 1978.
3. Leibovich, S., "Vortex Stability and Breakdown: Survey and Extension," *AIAA J*, Vol. 22, No. 9, September, 1984.
4. Peake, D., and Tobak, M., "Three-Dimensional Interactions and Vortical Flows with Emphasis on High Speeds," NASA Technical Memorandum 81169, 1980.
5. Zatoloka, V.V., Ivanyushkin, A.K., and Nikolayev, A.V., "Interference of Vortices with Shocks in Airscoops: Dissipation of Vortices," *Fluid Mechanics, Soviet Research*, Vol. 7, No. 4, July-August, 1978.
6. Cutler, A.D. and Levey, B.S., "Vortex Breakdown in a Supersonic Jet," AIAA-91-1815, Honolulu, HA, June, 1991.
7. Liu, C.H., "Admissible Upstream Conditions for Slender Compressible Vortices," AIAA-86-1093, May, 1986.
8. Mandella, M. and Bershader, D., "Quantitative Study of the Compressible Vortex: Generation, Structure, and Interaction with Airfoils," AIAA-87-0328, January, 1987.
9. Glotov, G.F., "Interference of Vortex Braid with Free-stream Shock Waves and Nonisobaric Jets," *Uchenyye Zapiski TsAGI*, Vol. XX, No. 5, pp 21-32, 1989.
10. Gostintsev, Yu.A., Zelentsov, V.V., Ilyukhin V.S., and Pokhil, P.F., "Structure of Underexpanded Supersonic Swirling Gas Jet," *Izv. AN SSSR, Mekhanika Zhidkosti i Gaza*, Vol. 4, No. 5, pp. 158-162, 1969.
11. Craven, A.H. and Alexander A.J., "An Investigation of Vortex Breakdown at Mach 2," CoA Note Aero-158, College of Aeronautics, Cranfield, 1963.
12. Metwally, O.M., Settles, G.S., and Horstman, C.C. "An Experimental Study of Shock/Vortex Interaction," AIAA-89-0082, January, 1989.
13. Metwally, O.M., "The Interaction of Supersonic Streamwise Vortex and a Normal Shock Wave," PhD Thesis, Dept. of Mechanical Engineering, Penn State Univ., August, 1989.
14. Délery, J., Horowitz, E., Leuchter, O., and Solignac, J.-L., "Fundamental Studies on Vortex Flows," *La Recherche Aerospatiale*, No. 1984-2.
15. Corpening, G. and Anderson, J., "Numerical Solutions to Three-Dimensional Shock Wave/Vortex Interaction at Hypersonic Speeds," AIAA-89-0674, January, 1989.
16. Kandil, O.A., Kandil H.A., and Liu, C.H., "Computation of Steady and Unsteady Compressible Quasi-Axisymmetric Vortex Flow and Breakdown," AIAA-91-0752, January, 1991.
17. Naughton, J.W., Cattafesta, L.N., and Settles, G.S., "A Miniature, Fast-Response, Five-Hole Probe for Supersonic Flowfield Measurements," AIAA-92-0266, January, 1992.
18. Deissler, R.G. and Perlmutter, M., "Analysis of the Flow and Energy Separation in a Turbulent Vortex," *J. Heat & Mass Transfer*, Vol. 1, pp. 173-91, 1960.
19. Cattafesta III, L. N., "An Experimental Investigation Of Shock/Wave Vortex Interaction," Ph.D. Thesis, Dept. of Mechanical Engineering, Penn State University, December, 1992.
20. Hoffmann, E. R. and Joubert, P. N., "Turbulent Line Vortices," *J. Fluid Mech.*, 16, pp. 395-411, 1963.

21. Délery, J., Pagan, D., and Solignac, J.L.,"On the Breakdown of the Vortex Induced by a Delta-Wing," ONERA T.P. 1987-105, April, 1987.
22. Hall, M. G., "Vortex Breakdown," *Annual Review of Fluid Mechanics,* vol. 4, pp. 195-218, 1972.

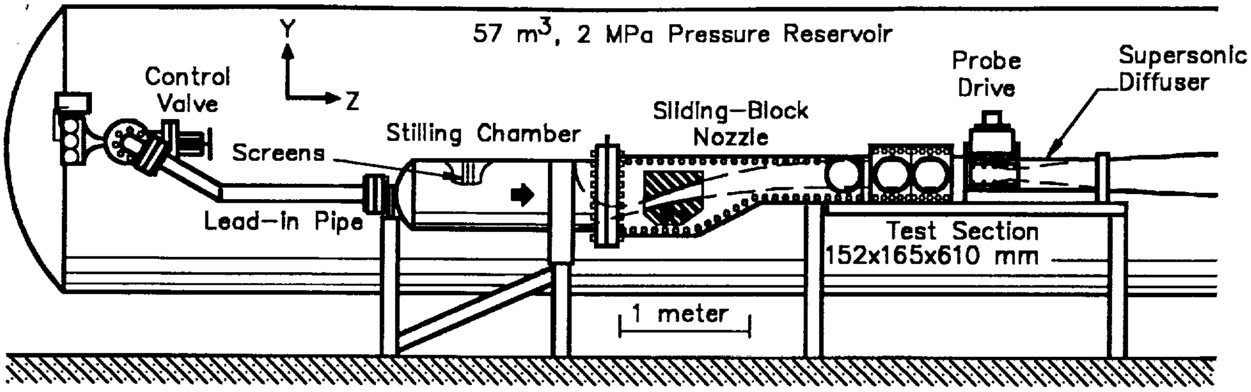

Figure 1(a). The Penn State Supersonic Wind Tunnel Facility.

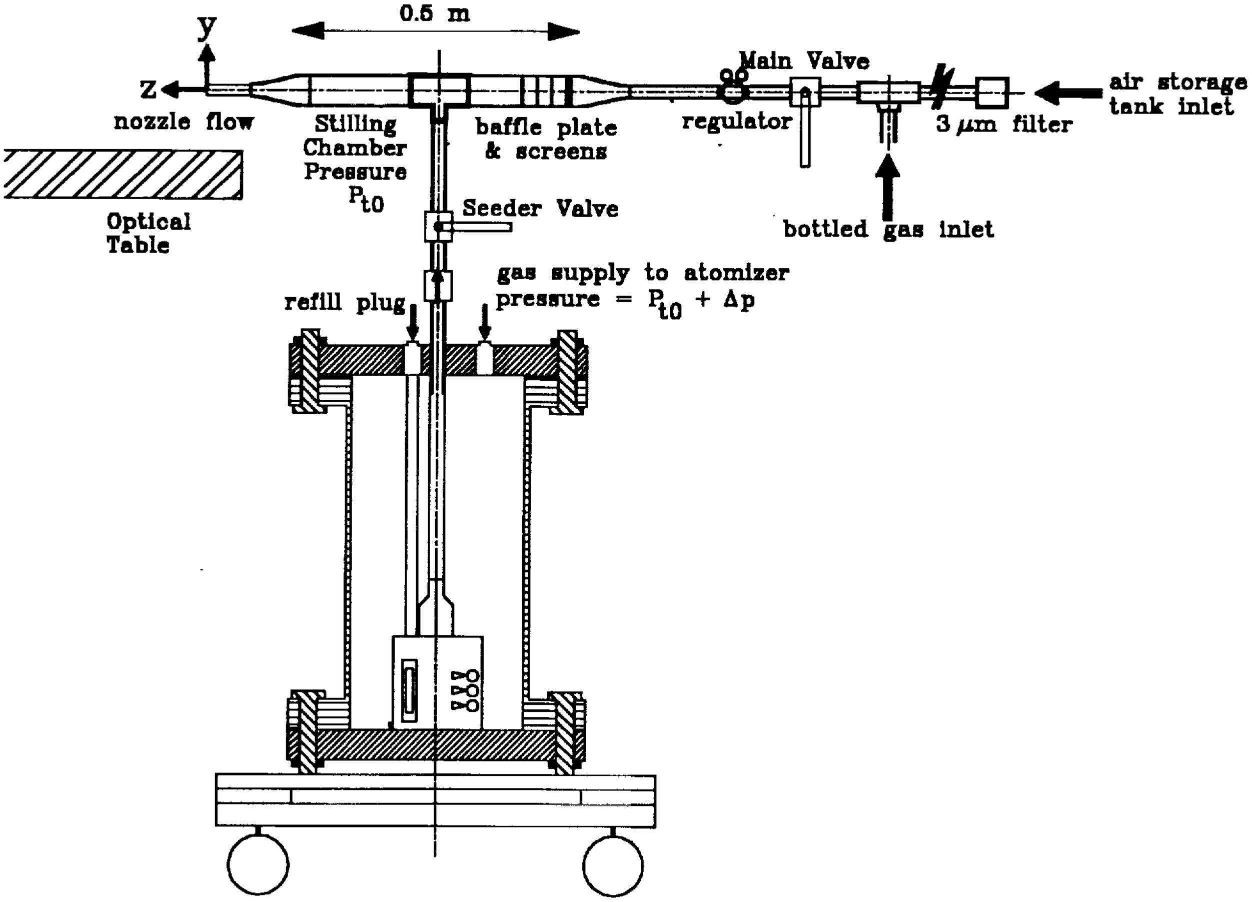

Figure 1(b). The Penn State Gas Dynamics Laboratory Freejet Facility.

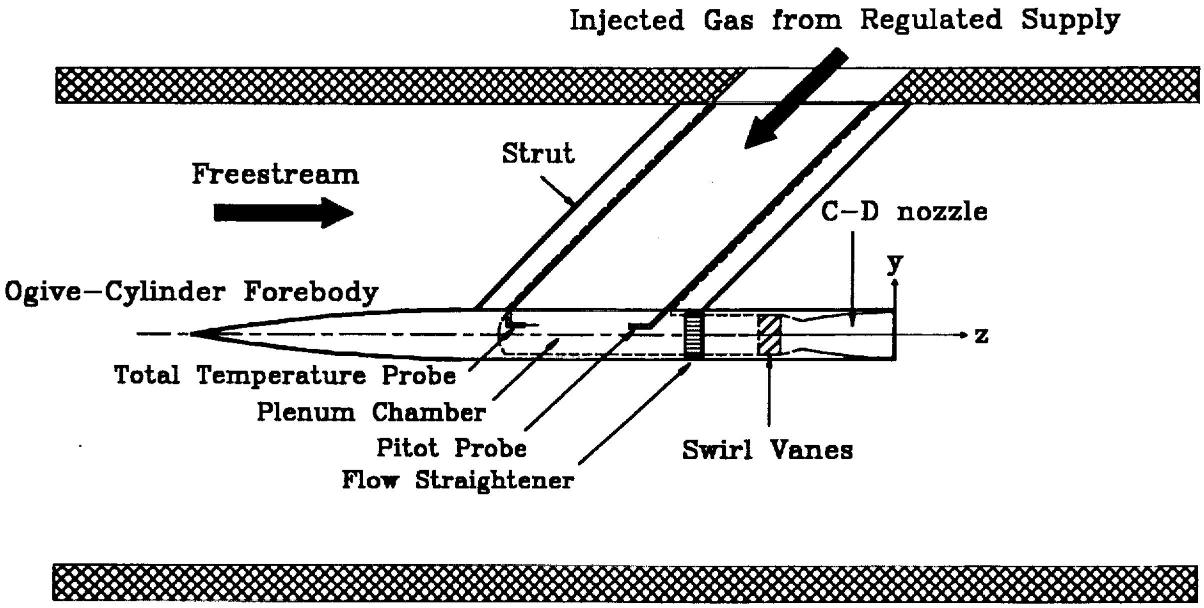

Figure 2. The supersonic streamwise vortex generator.

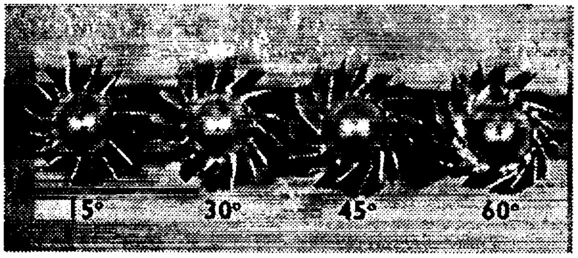

Figure 3. The swirl vanes.

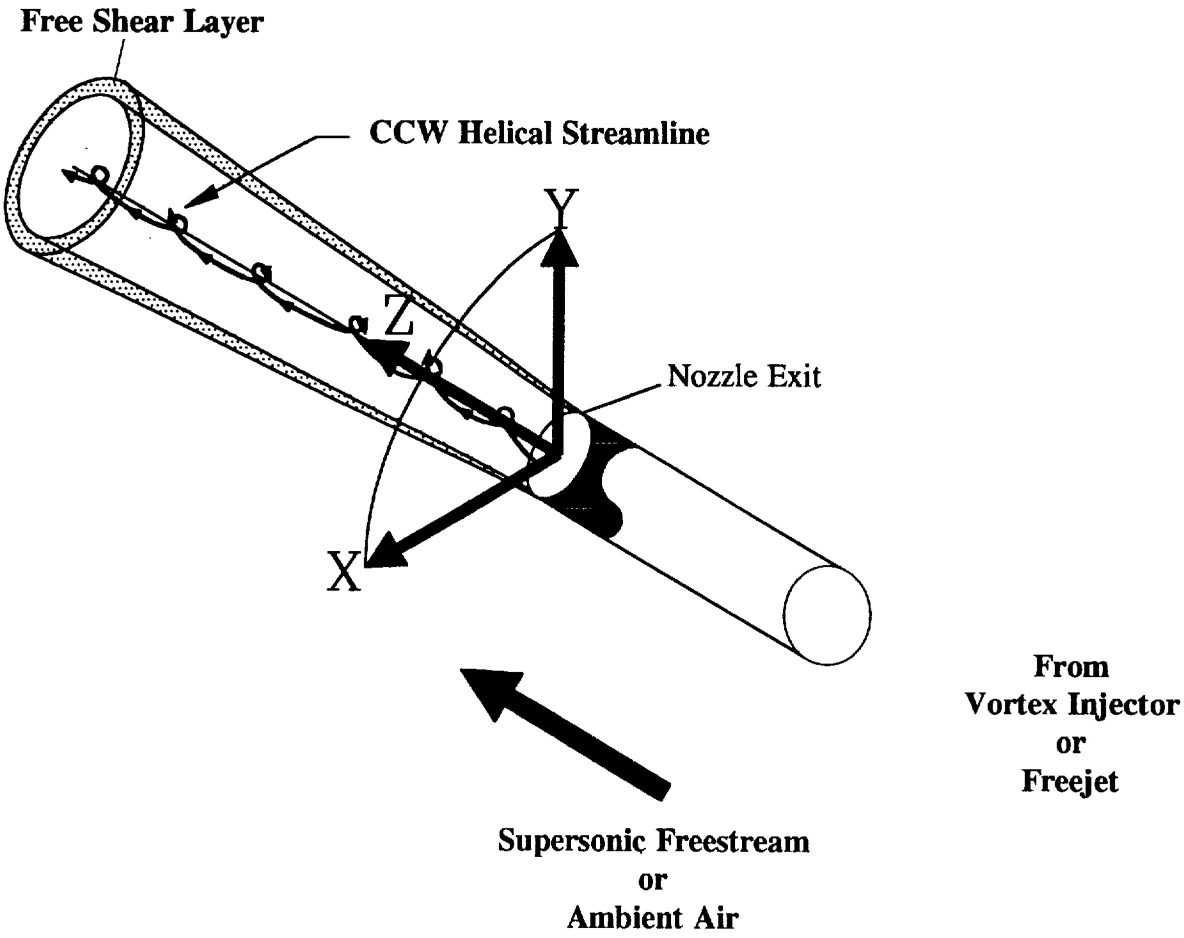

Figure 4. Schematic of a supersonic streamwise vortex.

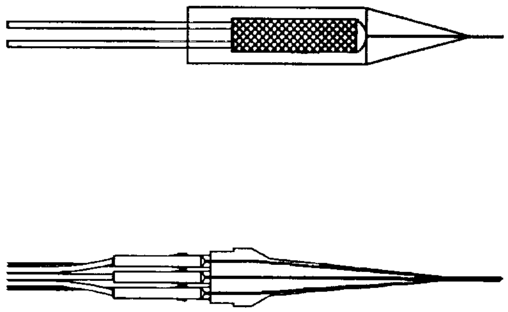

Total Temperature Probe

Type K Thermocouple
Microdisc Junction
Junction Size: 2.5 μm thick 20 μm diam.
Spatial Resolution: < 0.2 mm
Time Response to Step Input: 20 msec

Five-Hole Probe

Piezoresistive Transducers
Sensitivity: 6 mv/psi
Compensated Temp. Range: -54 to 121 °C
Spatial Resolution: < 1 mm
Time Response to Step Input: 20 msec

Figure 5. Details of the T_t and Five-Hole probes.

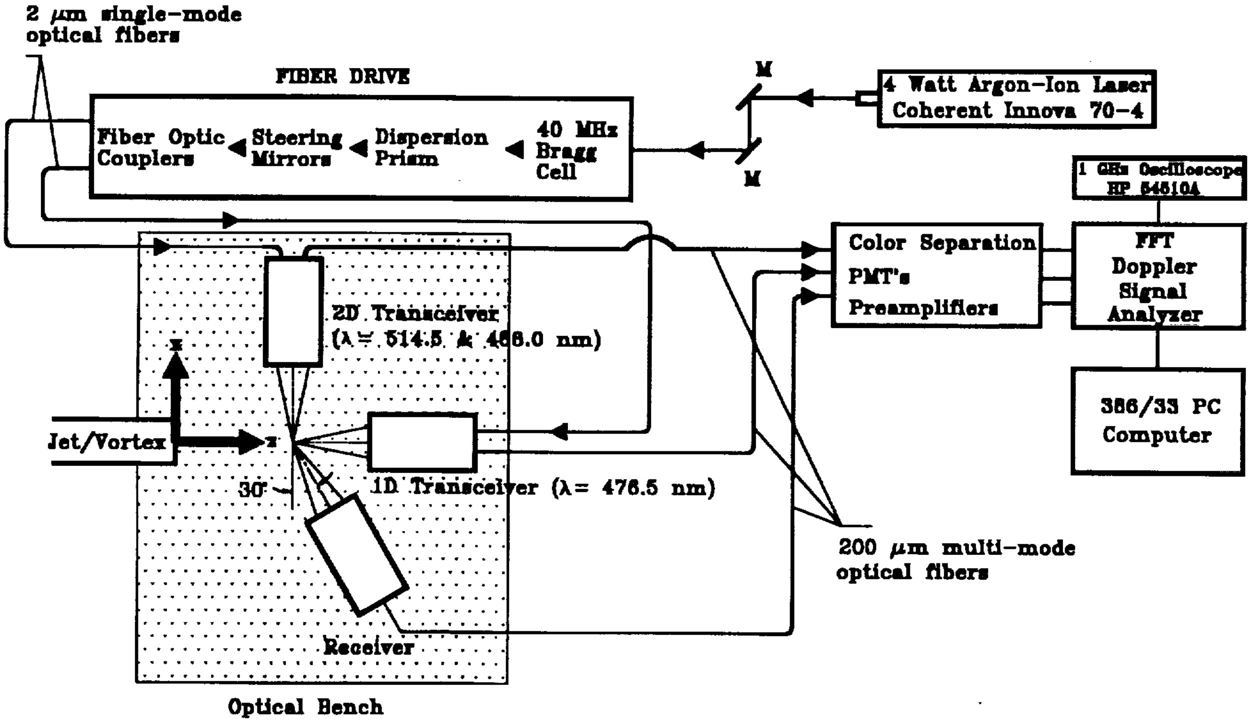

Figure 6. The Laser Doppler Velocimeter system.

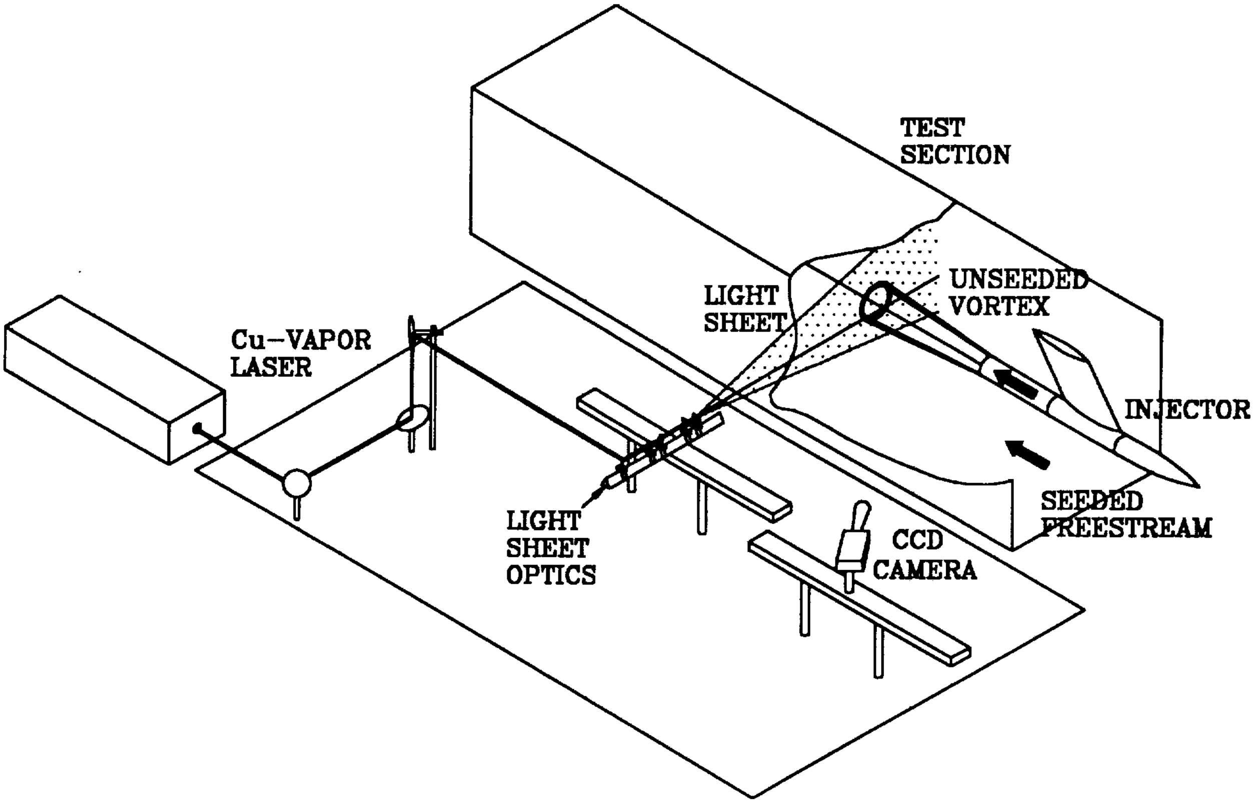

Figure 7. The Planar Laser Scattering method.

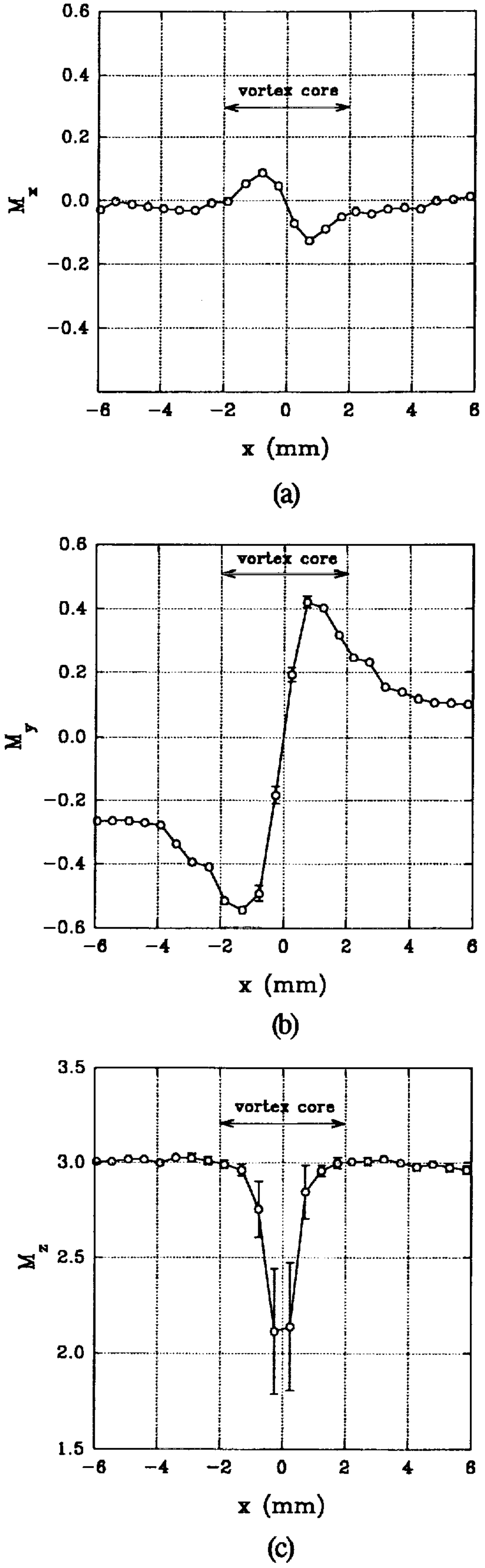

(a)

(b)

(c)

Figure 8. Component Mach number distributions of a Mach 3, 30°-vane vortex. (a) radial; (b) tangential; and (c) axial.

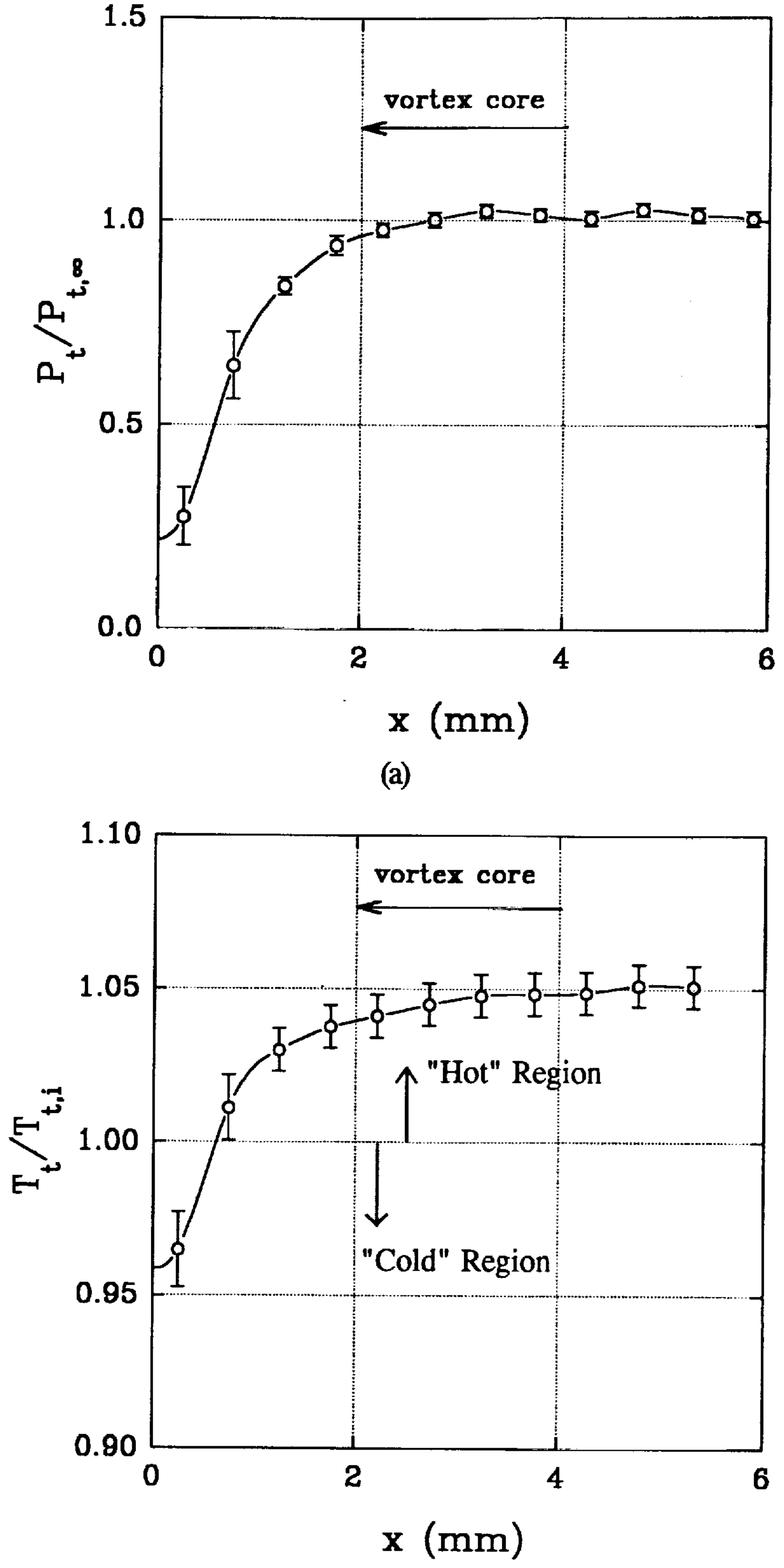

(a)

(b)

Figure 9. (a) Total pressure and (b) Total temperature distributions of a Mach 3, 30°-vane vortex.

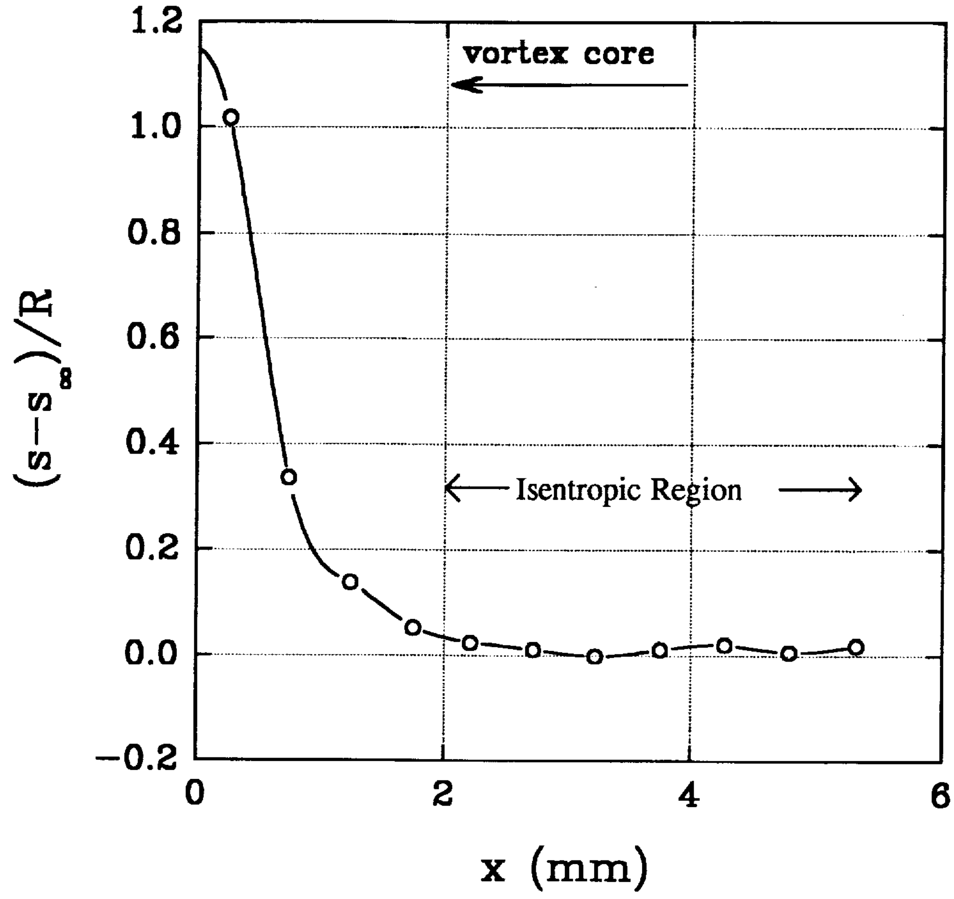

Figure 10. Entropy distribution of a Mach 3, 30°-vane vortex.

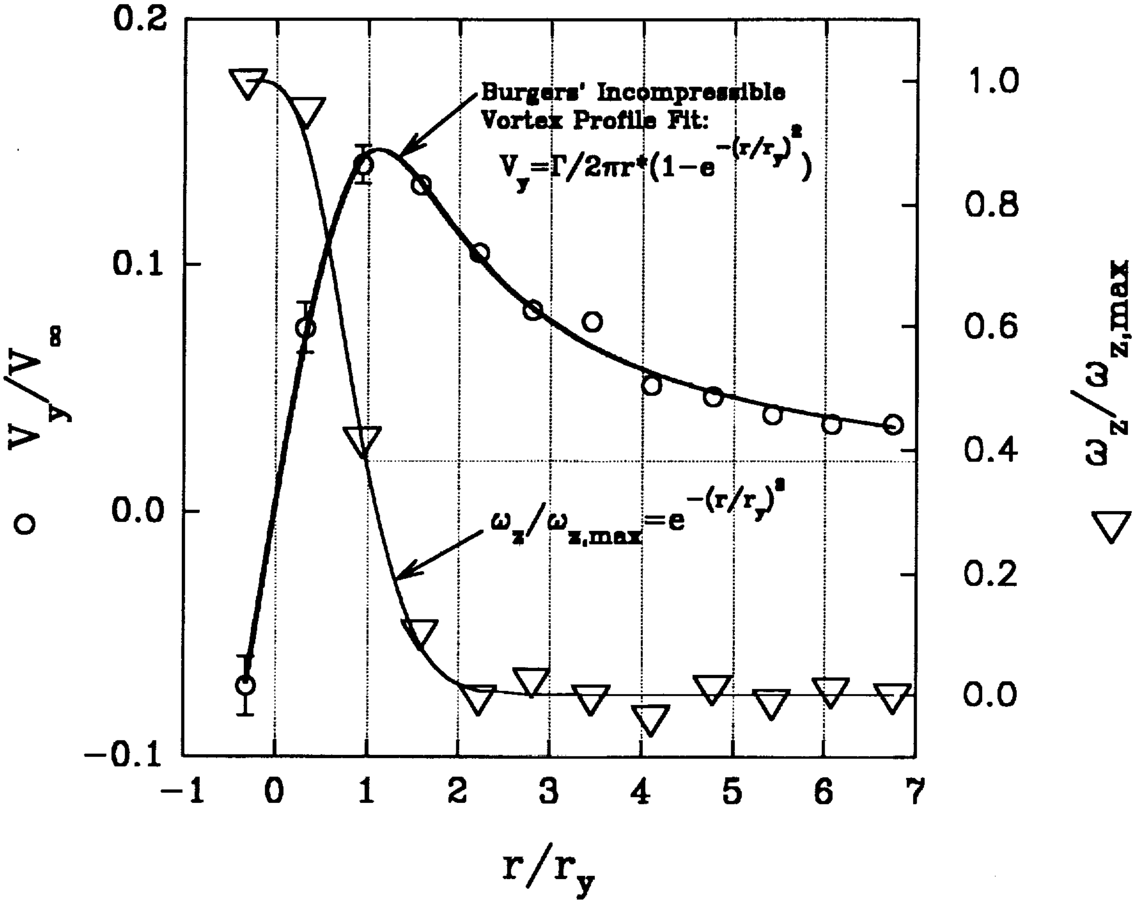

Figure 11. Tangential Velocity and Streamwise Vorticity Distributions of a Mach 3, 30°-Vane Vortex.

$K = rV_t$ r_1 = location where V_t is a maximum

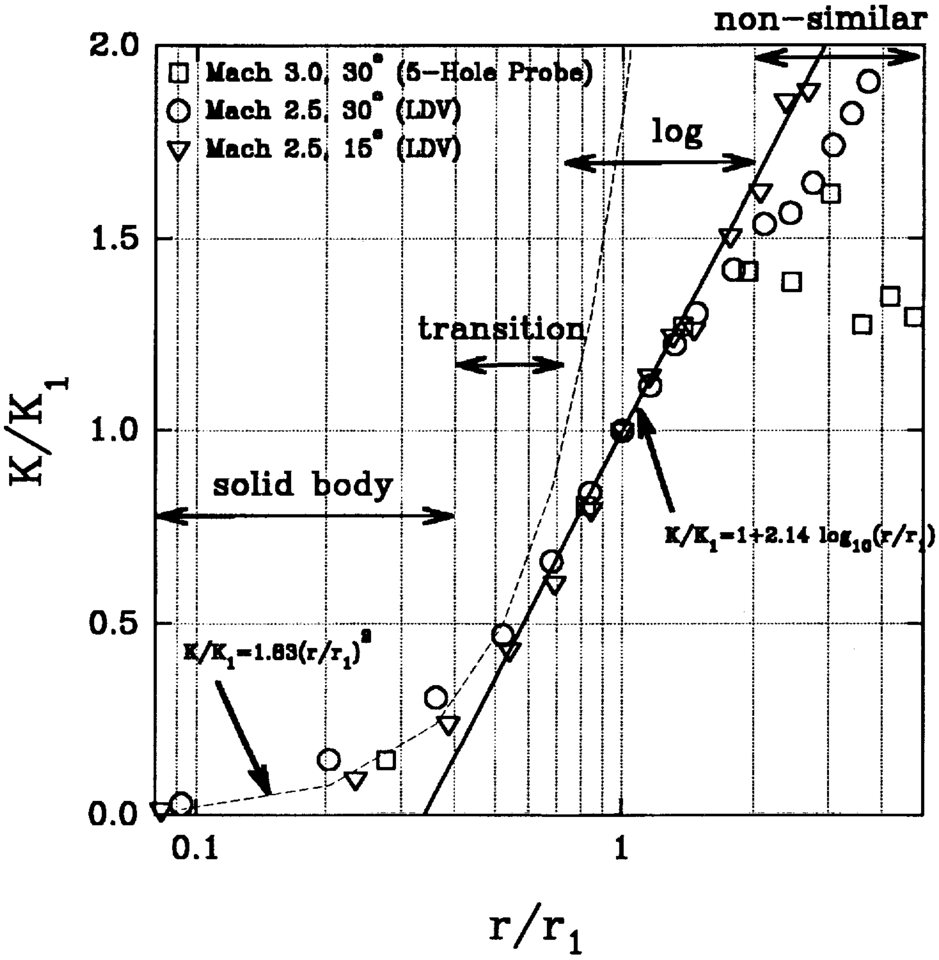

Figure 12. The self-similar circulation distribution.

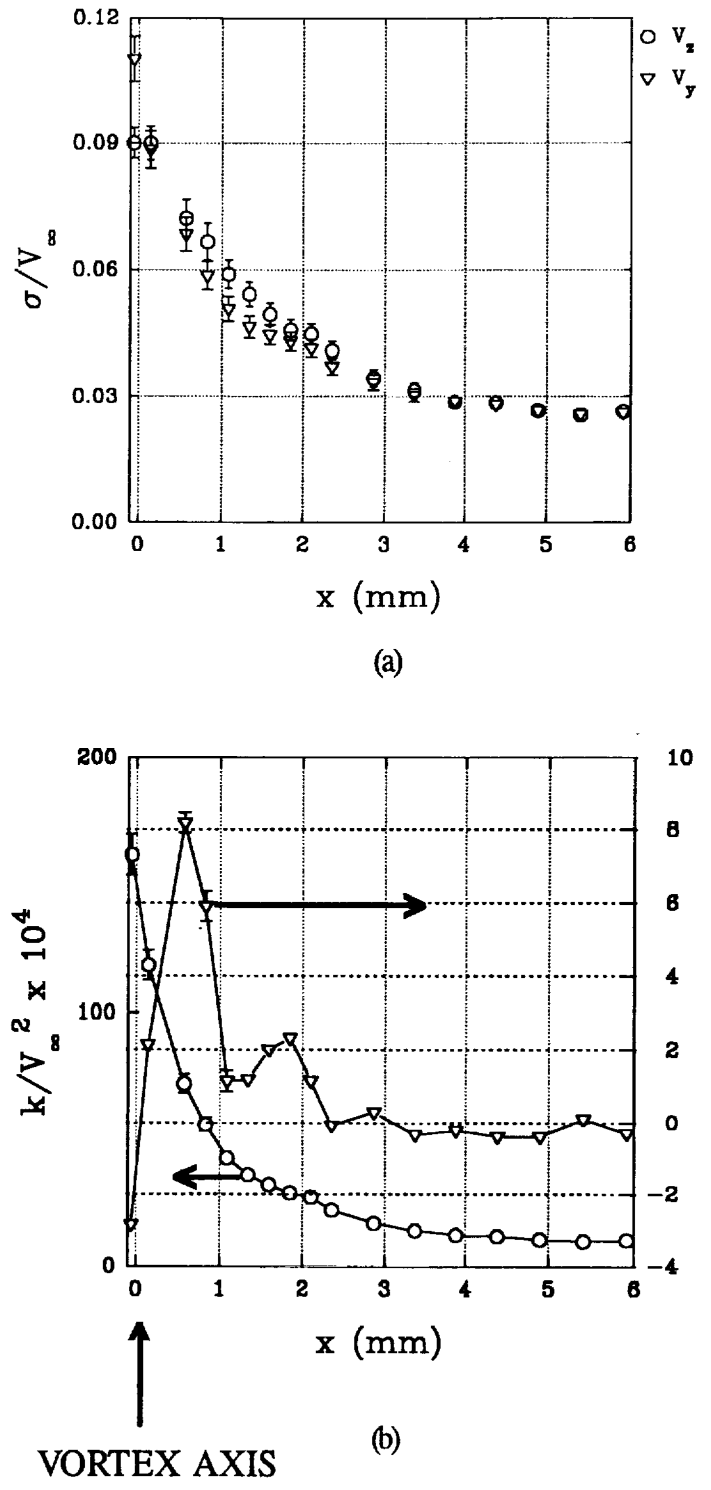

Figure 13. Turbulent structure of the Mach 2.5, 30°-vane vortex. (a) rms velocities; (b) turbulent kintic energy and axial-radial Reynolds stress.

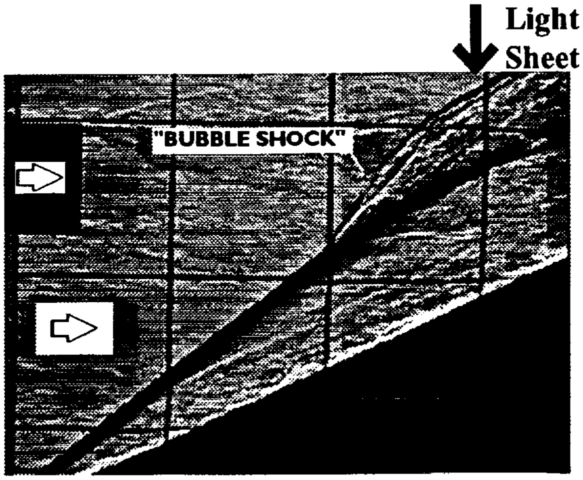

Figure 14. Schlieren image of an oblique shock/vortex interaction. $M_{vortex} = 2.5$, $M_{freestream} = 4.0$, 60° vanes, 25° wedge.

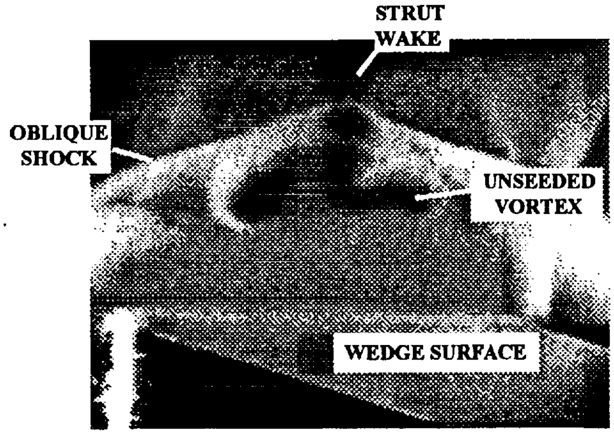

Figure 15. Time-averaged PLS image of an oblique shock/vortex interaction. $M_{vortex} = 2.5$, $M_{freestream} = 4.0$, 60° vanes, 25° wedge.

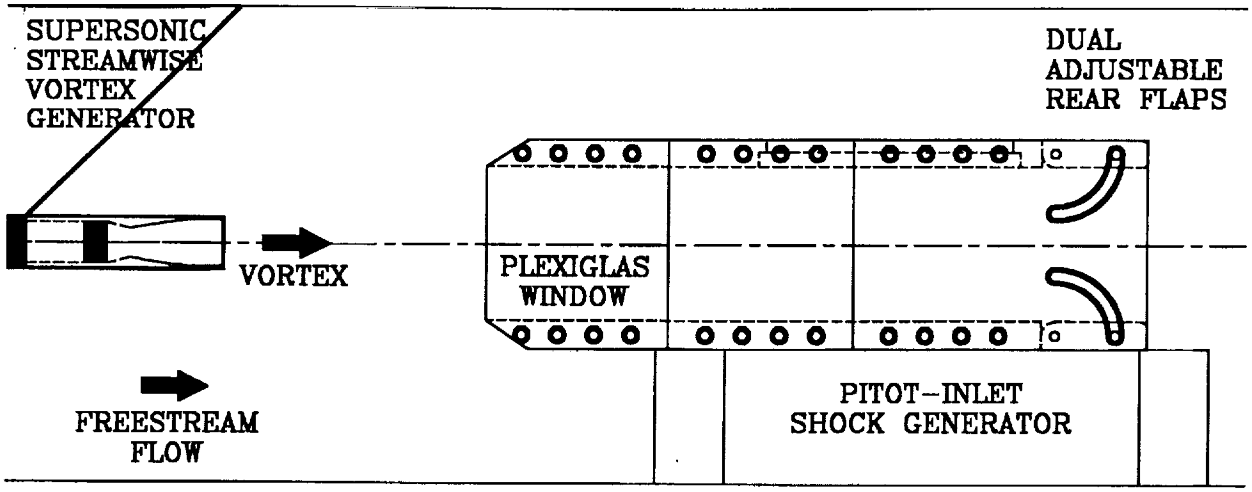

Figure 16. Schematic of pitot-inlet normal shock generator.

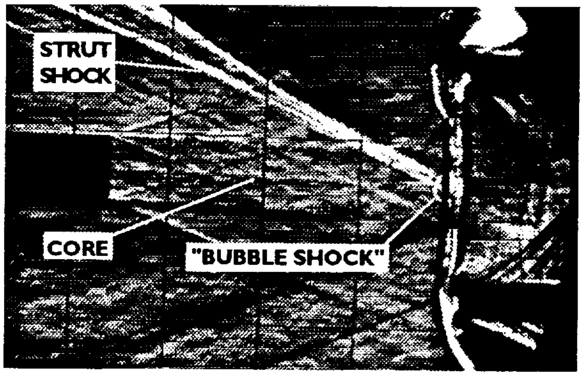

Figure 17. Schlieren image of a weak shock/vortex interaction at Mach 2.5 (15° vanes).

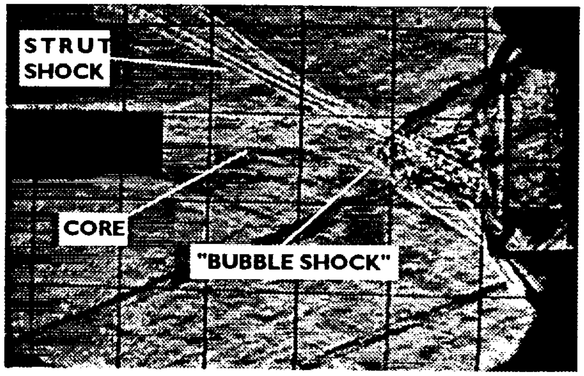

Figure 18. Schlieren image of a strong shock/vortex interaction at Mach 2.5 (30° vanes).

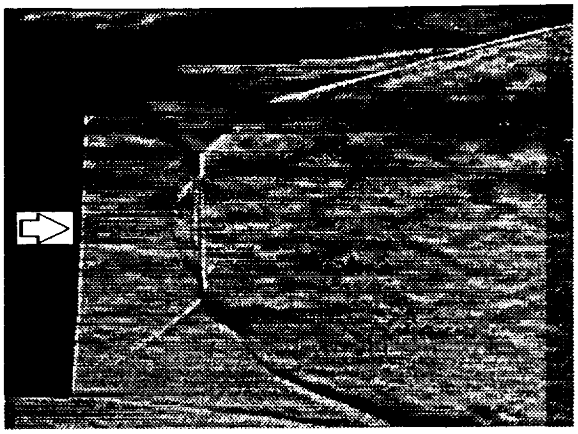

Figure 19. Schlieren image of a weak shock/vortex interaction for the overexpanded Mach 2.5 nozzle case. 15° vanes.

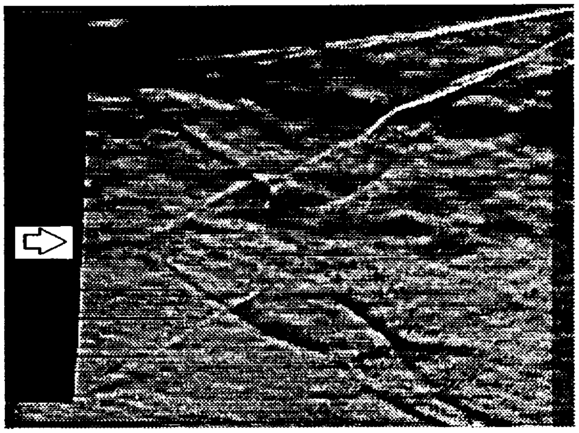

Figure 20. Schlieren image of a strong shock/vortex interaction for the overexpanded Mach 2.5 nozzle case, 30° vanes.

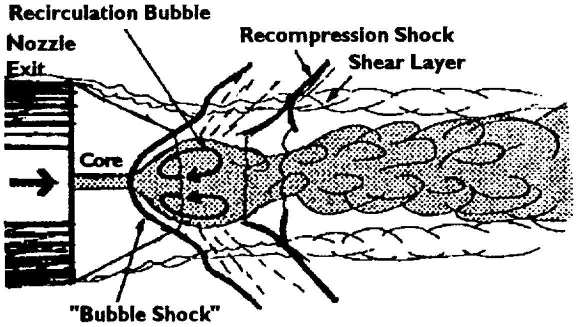

Figure 21. Schematic of a model for the strong shock/vortex interaction from Metwally[12,13].

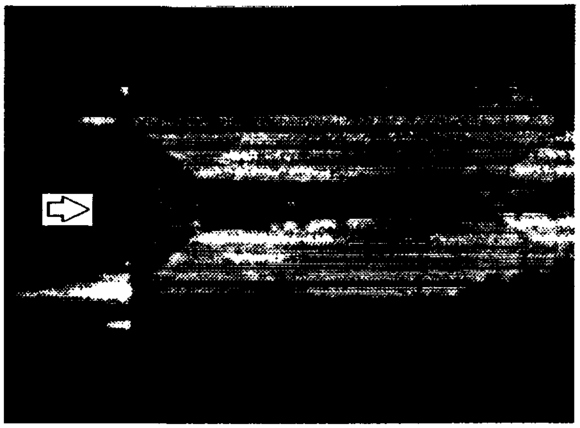

Figure 22. Instantaneous PLS image of a Mach Disc in a Mach 2.5 freejet.

Figure 23. Instantaneous PLS image of a weak SWVI in an overexpanded Mach 2.5 freejet. 15° vanes.

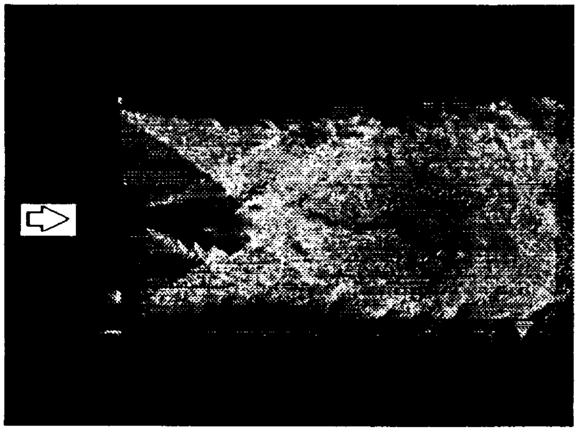

Figure 24. Instantaneous PLS image of a strong SWVI in an overexpanded Mach 2.5 freejet. 30° vanes.

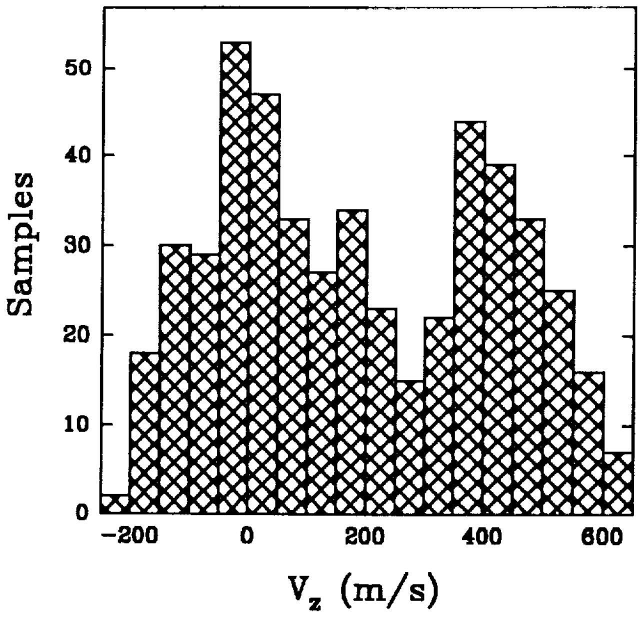

Figure 25. Histogram of LDV measurements in the heart of the strong SWVI.

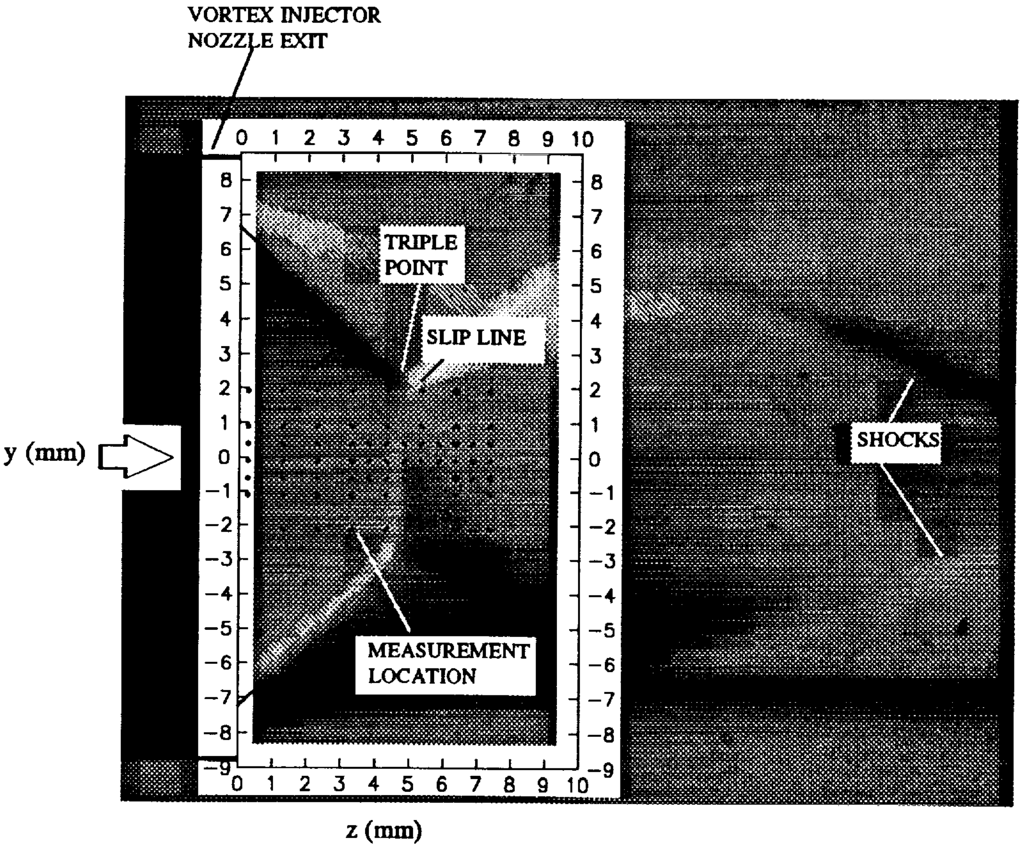

Figure 26. A grid of the LDV measurement locations of the weak overexpanded-nozzle SWVI superimposed on a time-averaged horizontal knife-edge schlieren image of the interaction.

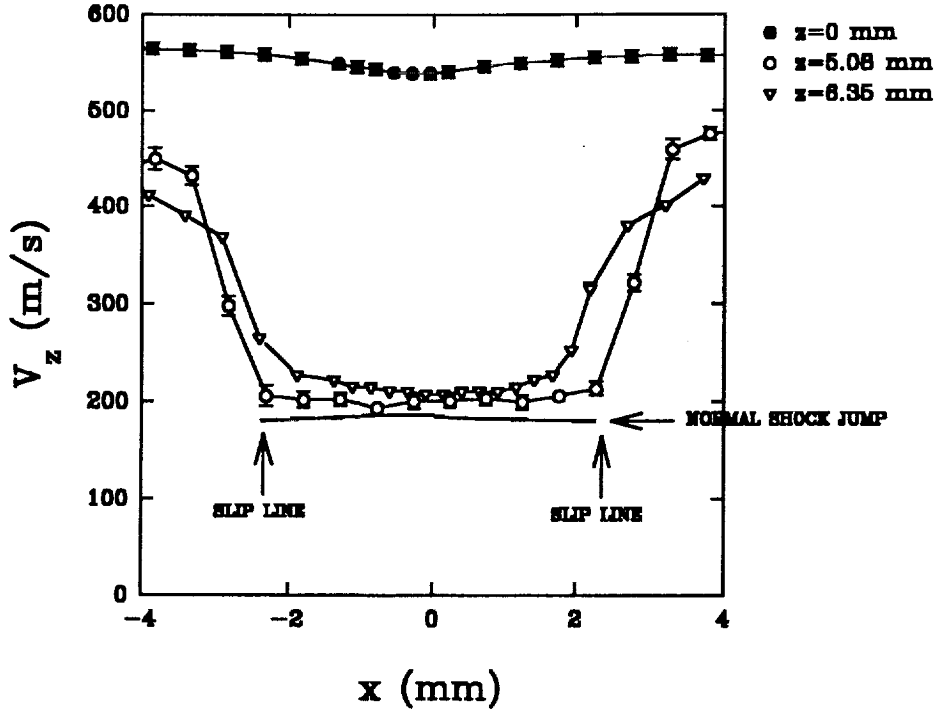

Figure 27. LDV measurements of axial velocity for the weak SWVI.

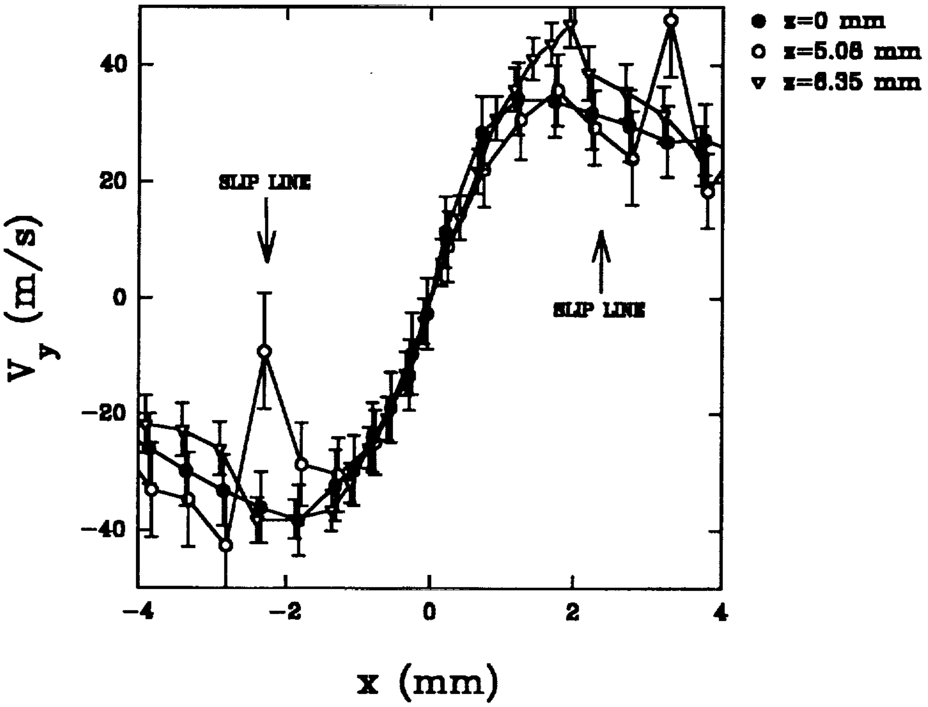

Figure 28. LDV measurements of tangential velocity for the weak SWVI.

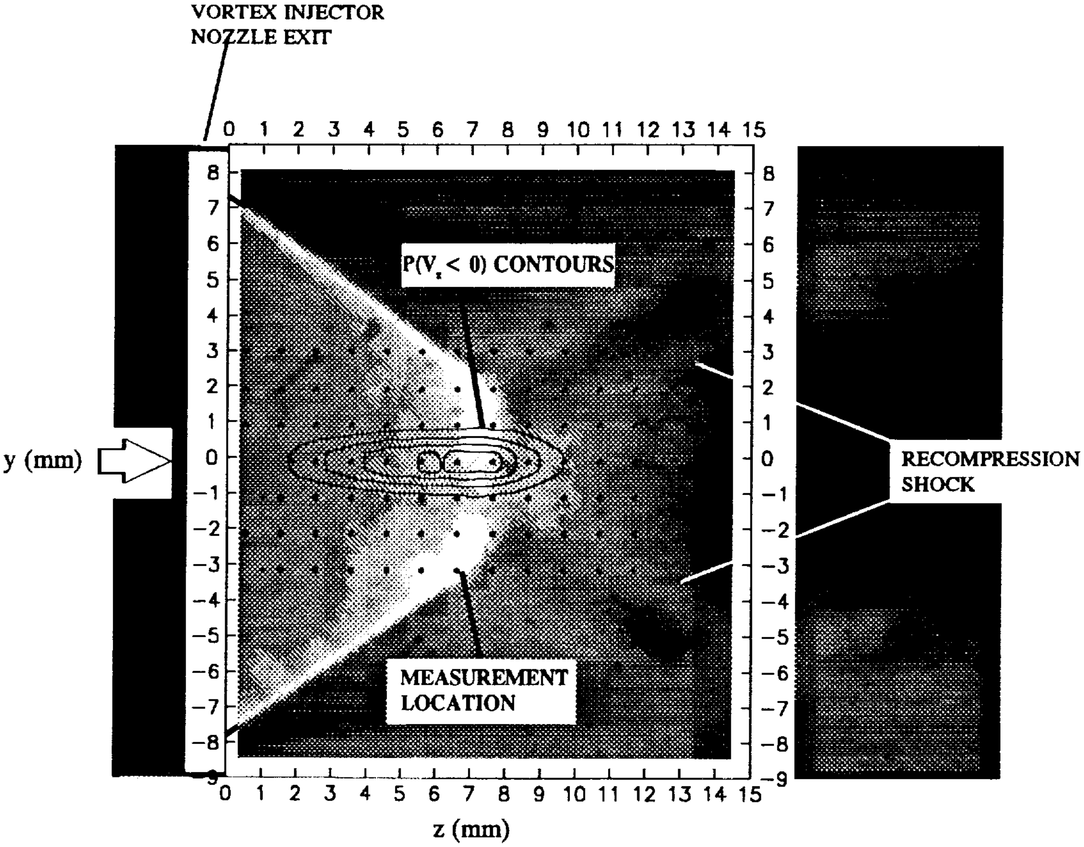

Figure 29. A grid of the LDV measurement locations and $P(V_z < 0)$ contours of the strong overexpanded-nozzle SWVI (small Mach-disc case) superimposed on a time-averaged vertical knife-edge schlieren image of the interaction.

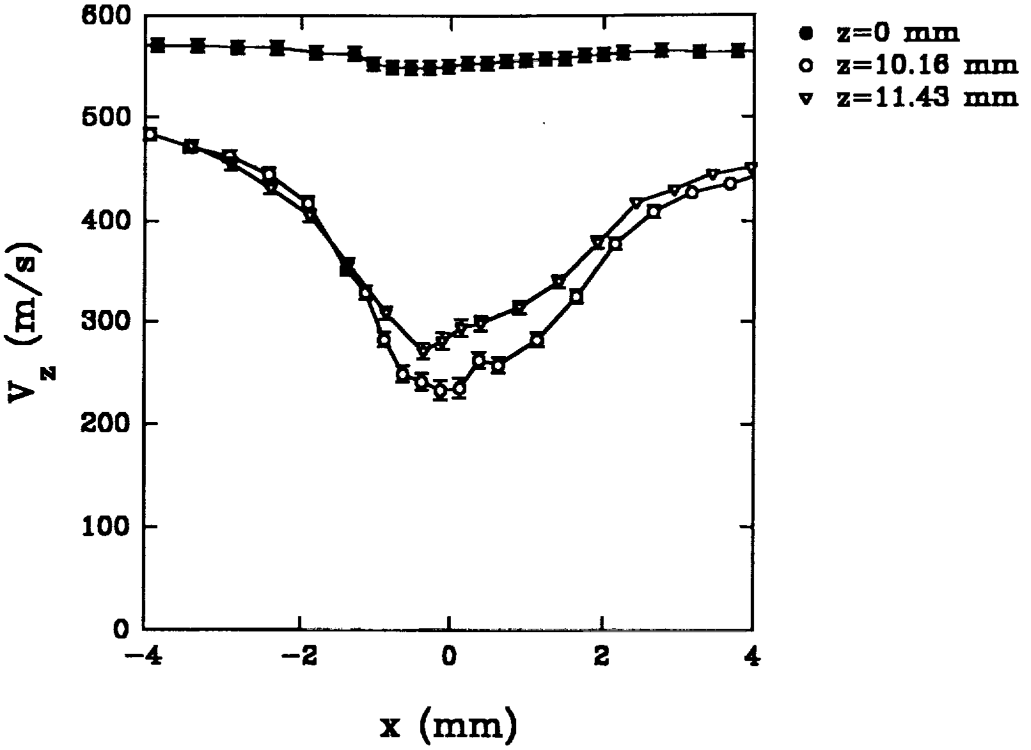

Figure 30. LDV measurements of axial velocity for the strong SWVI (small Mach-disc case).

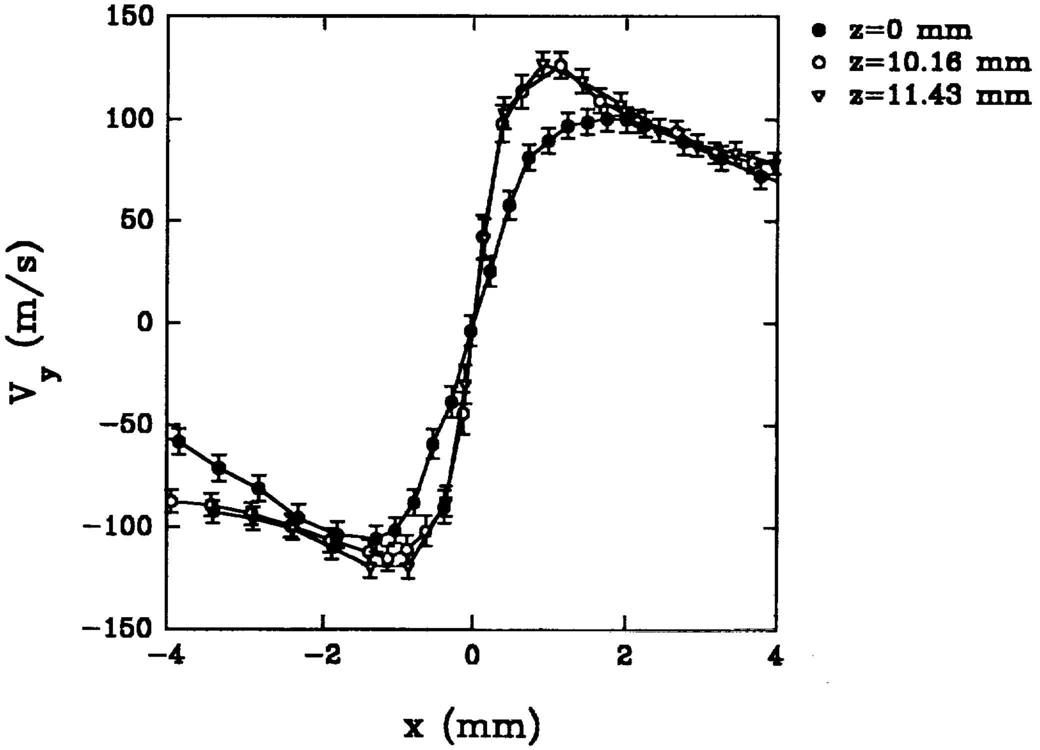

Figure 31. LDV measurements of tangential velocity for the strong SWVI (small Mach-disc case).

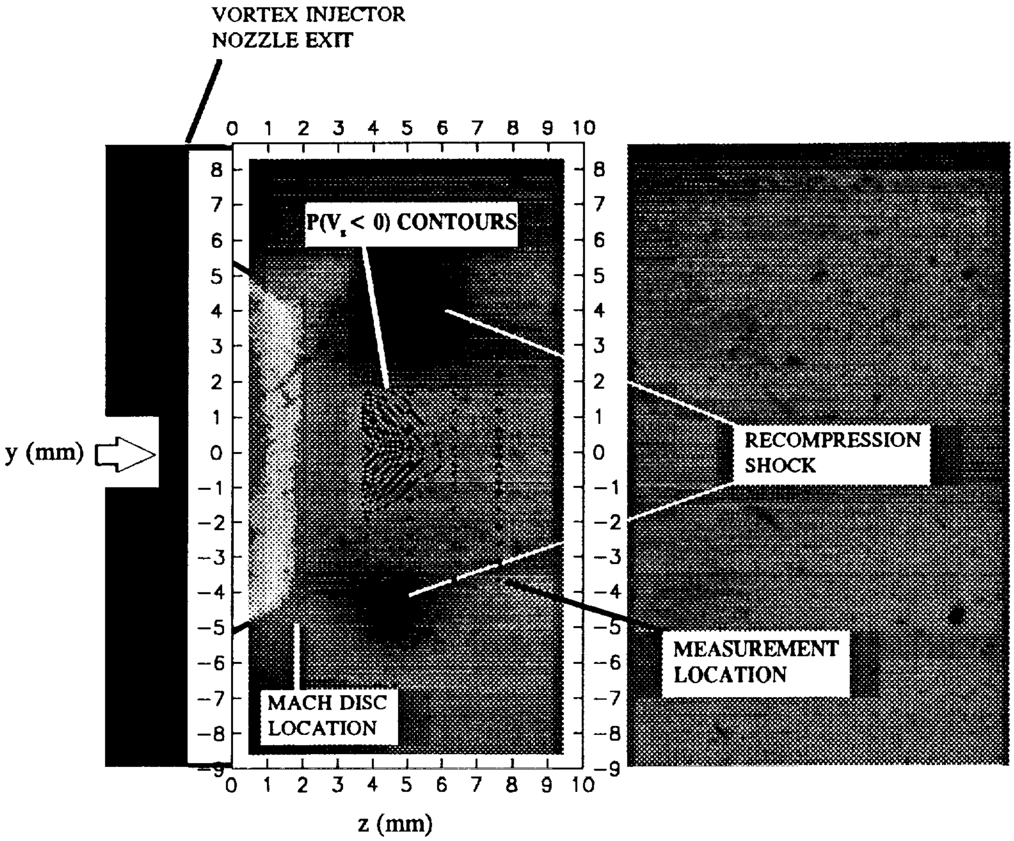

Figure 32. A grid of the LDV measurement locations and P(V_z < 0) contours of the strong overexpanded-nozzle SWVI (large Mach-disc case) superimposed on a time-averaged vertical knife-edge schlieren image of the interaction.

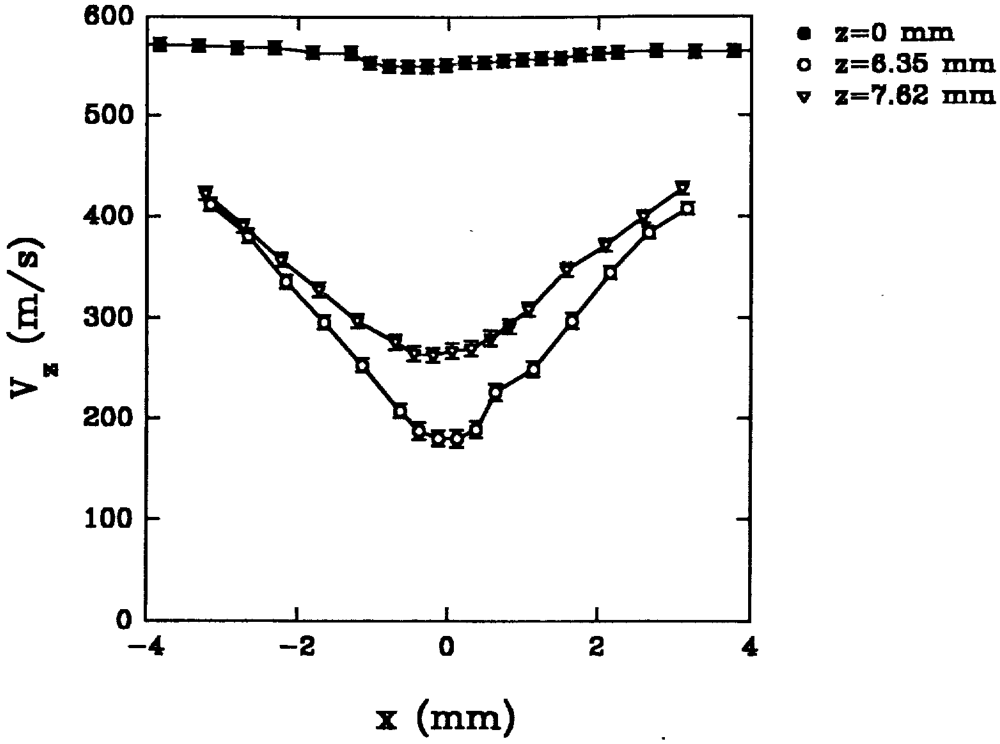

Figure 33. LDV measurements of axial velocity for the strong SWVI (large Mach-disc case).

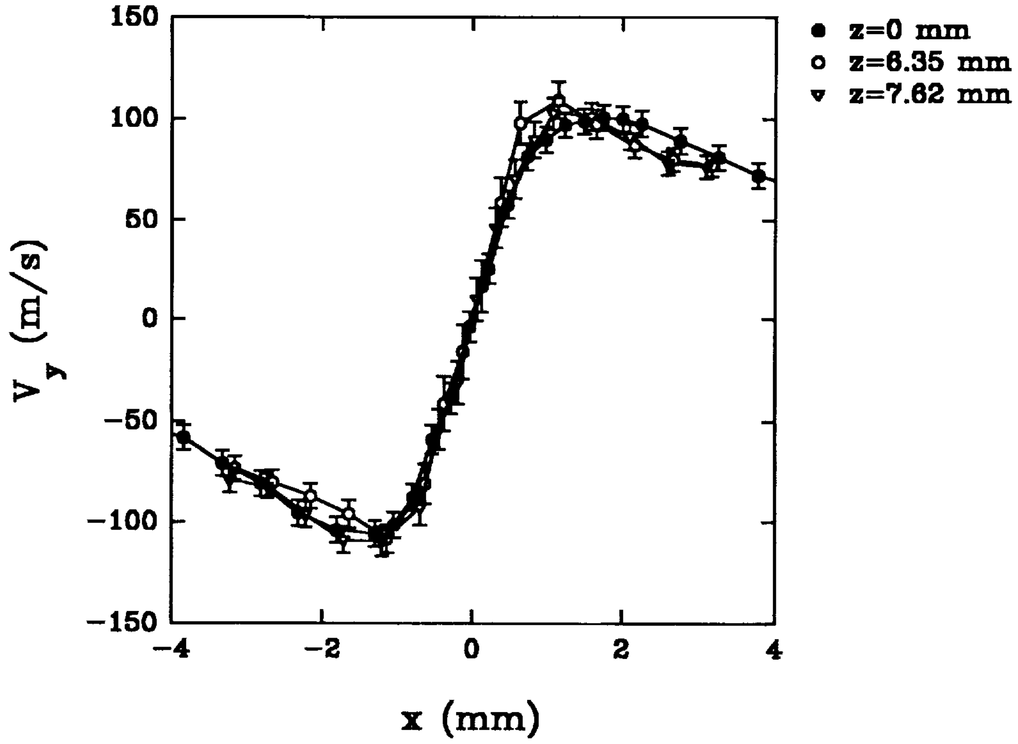

Figure 34. LDV measurements of tangential velocity for the strong SWVI (large Mach-disc case).

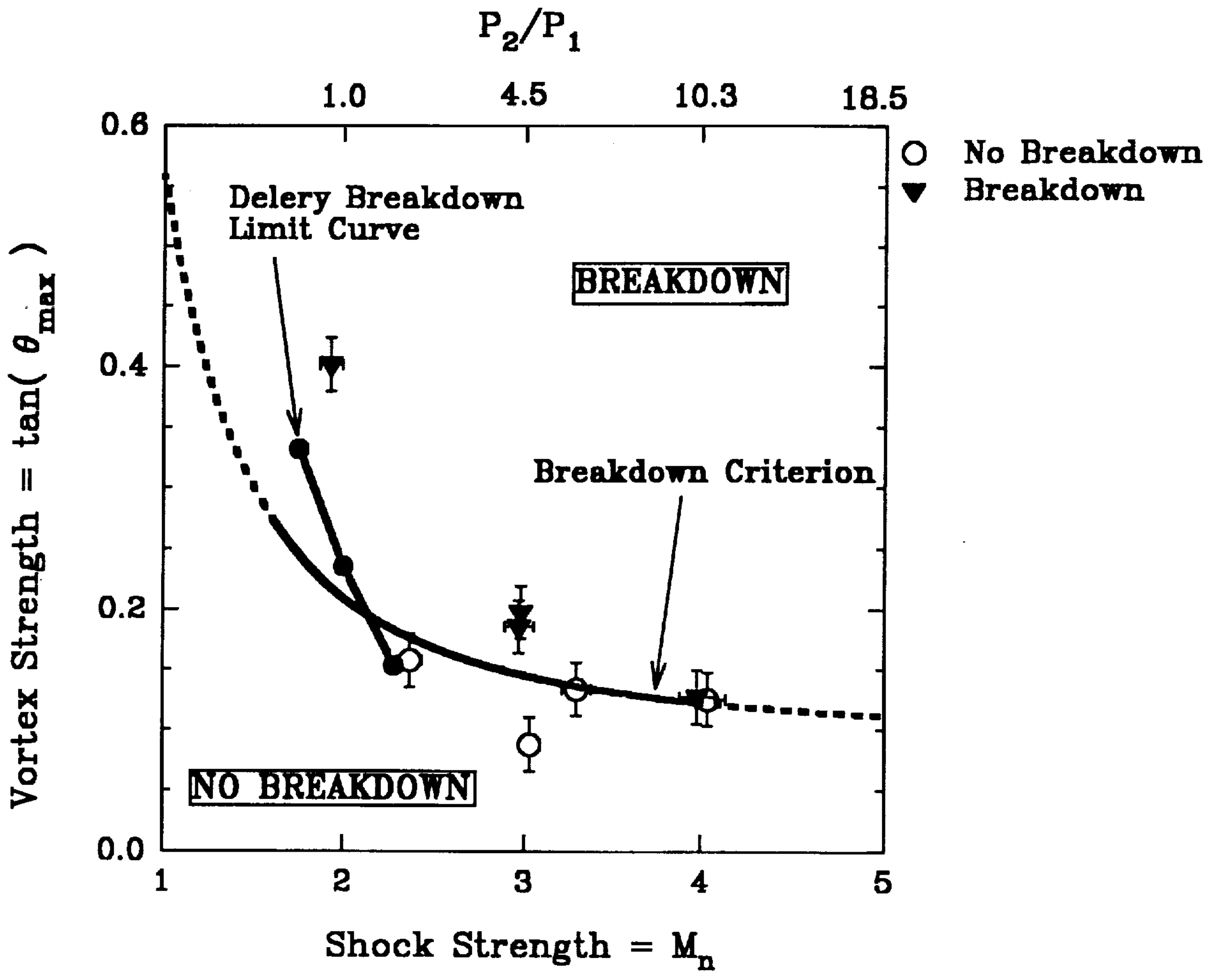

Figure 35. The supersonic vortex breakdown limits curve.

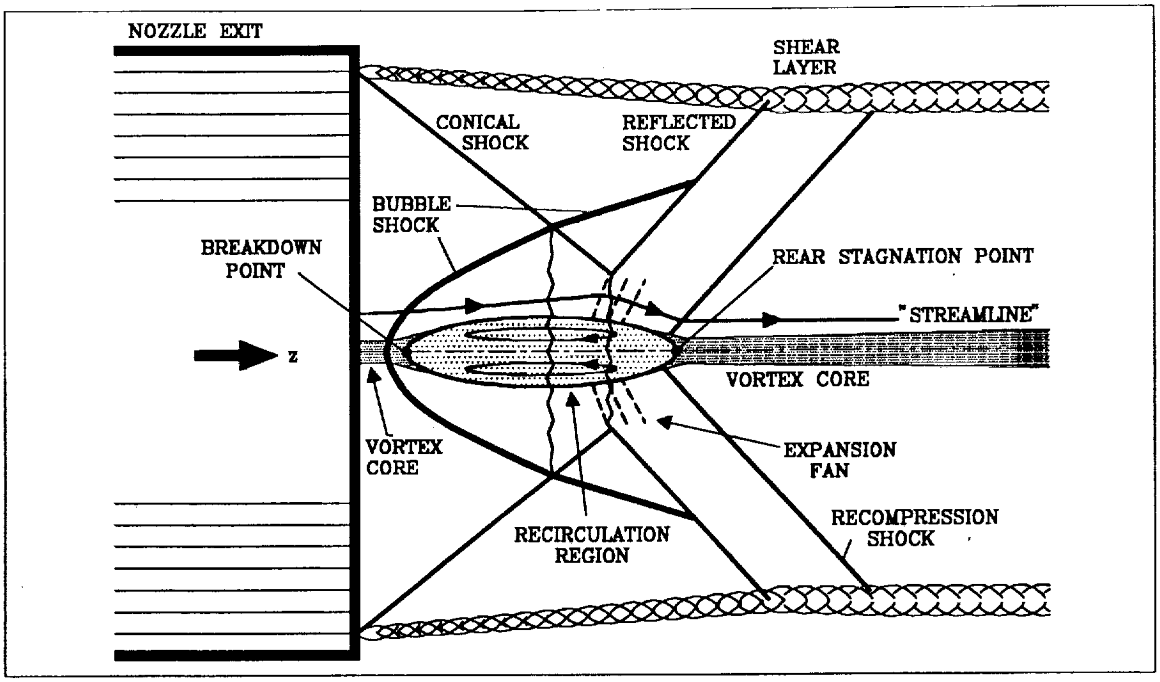

(a) An updated model of the strong SWVI for the small Mach-disc case.

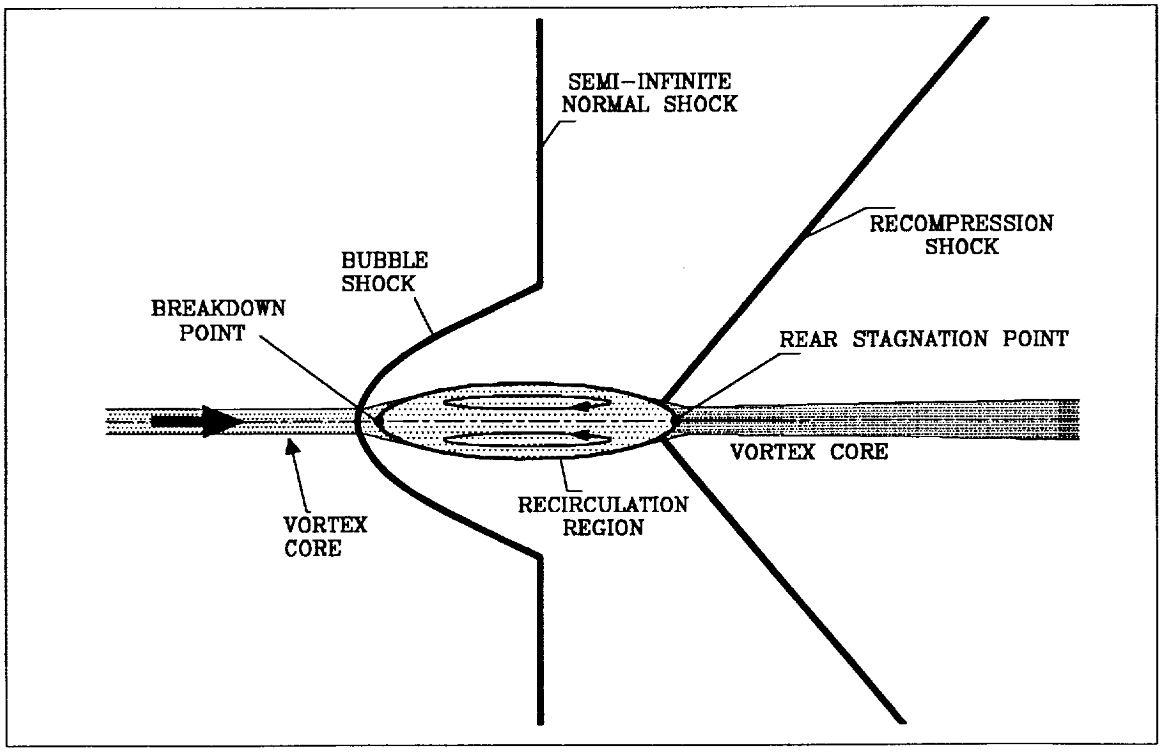

(b) A model of the strong SWVI for the semi-infinite normal shock case.

Figure 36. Models of the strong shock wave/vortex interaction.